AD-A071 419 MARYLAND UNIV COLLEGE PARK DEPT OF AEROSPACE ENGINEERING F/G 20/4
INVESTIGATION OF TRANSONIC GAS FLOWS (ANALYTICAL AND NUMERICAL --ETC(U)
MAR 79 O BELOTSERKOVSKII N00014-79-M-0022
UNCLASSIFIED AE-79-2 NL

1 OF 1
AD A071419

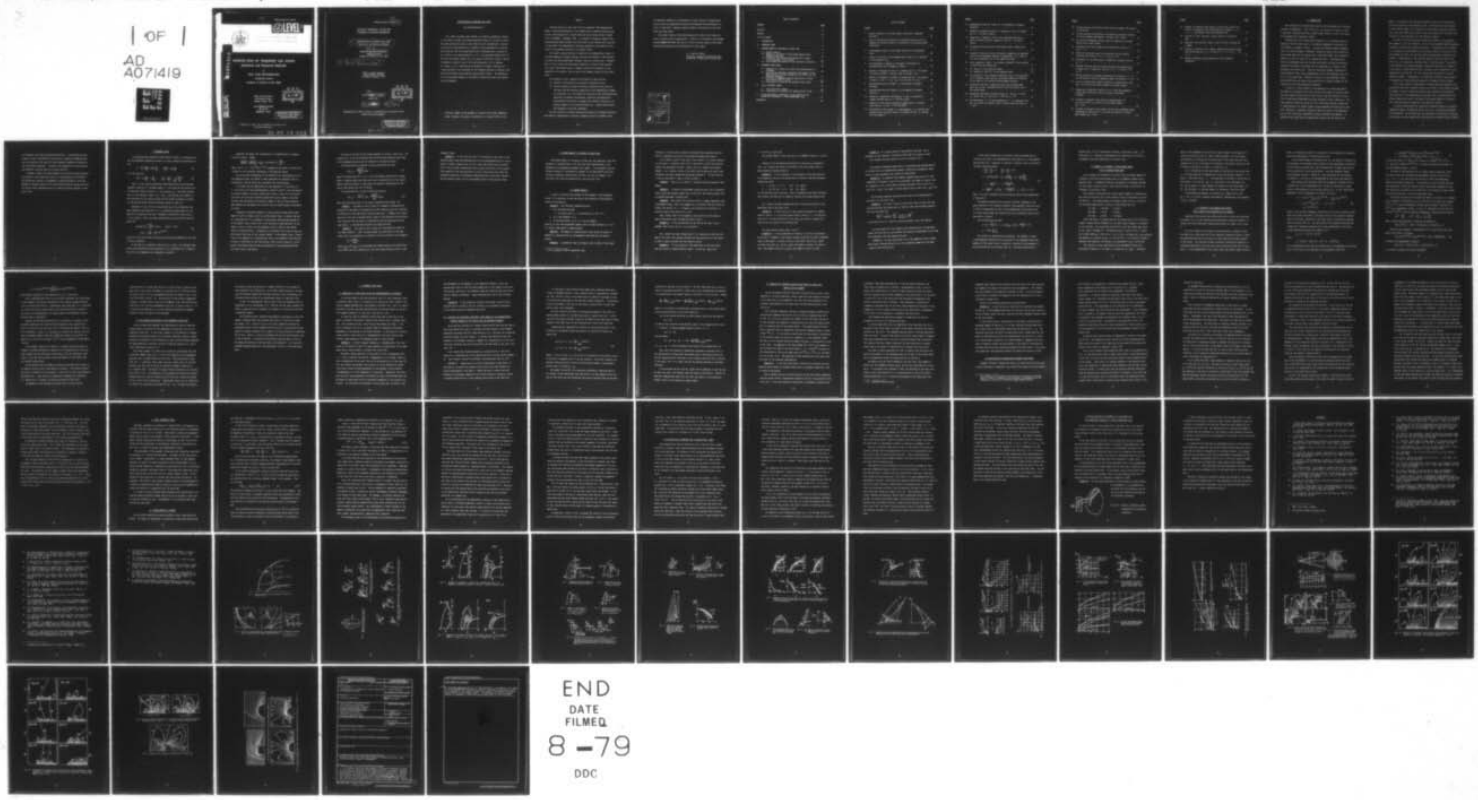

END
DATE FILMED
8-79
DDC

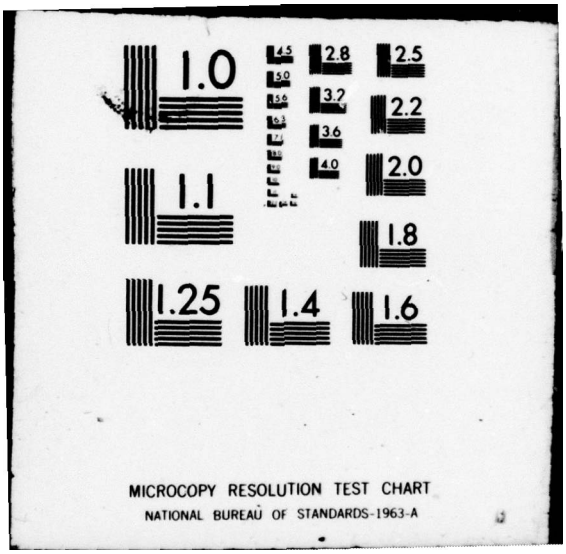
1.0
1.1
1.25
1.4
1.6
1.8
2.0
2.2
2.5
2.8
3.2
3.6
4.0
4.5
5.0
5.6
MICROCOPY RESOLUTION TEST CHART
NATIONAL BUREAU OF STANDARDS-1963-A

Technical Report No. AE-79-2

(12) LEVEL II

University of Maryland, College Park
Department of Aerospace Engineering

INVESTIGATION OF TRANSONIC GAS FLOWS
(Analytical and Numerical Methods)

by

PROF. OLEG BELOTSERKOVSKII
Computing Center
Academy of Sciences of the USSR

Office of Naval Research
Fluid Dynamics Program
Arlington, Virginia 22217

Contract N00014-79-M-0022
NR 061-262
MARCH, 1979

(14) Technical Report No. AE-79-2

UNIVERSITY OF MARYLAND, COLLEGE PARK
DEPARTMENT OF AEROSPACE ENGINEERING

(6) # INVESTIGATION OF TRANSONIC GAS FLOWS (Analytical and Numerical Methods).

(10) by

PROFESSOR OLEG BELOTSERKOVSKII
Computing Center
Academy of Sciences of the USSR

(9) Final technical rept.,

Office of Naval Research
Fluid Dynamics Program
Arlington, Virginia 22217

(15) Contract N00014-79-M-0022

NR 061-262

(11) Mar[redacted]79

(12) 73p.

401 860

INVESTIGATION OF TRANSONIC GAS FLOWS

O.M. Belotserkovskii *

This report considers some problems of transonic gasdynamics related to the theory of planar and three-dimensional flows of a perfect gas which have been worked out mainly by the author and his collaborators. Results of analytical investigations of a number of exact properties of solutions which describe the flow around bodies with a detached shock, obtained by E.G. Shifrin, O.M. Belotserkovskii, et al., are presented without proof in the form of theorems (proofs are to be found in the papers cited). Results of numerical solutions (due to O.M. Belotserkovskii, Yu. M. Davidov, F.D. Popov, et al.), obtained by the methods of integral relations and "large particles", are presented for the complete problem of transonic flow around blunt bodies whose profiles possess sharp corners. The boundaries of distinct minimal domains of influence in mixed flow about blunt bodies are also examined.

* Professor, Member of the Academy of Sciences of the USSR, Computing Center, Academy of Sciences, 40 Vavilova St., Moscow V-333, U.S.S.R.

PREFACE

Selected results of this report and its companion "New Computational Models in Continuum Mechanics," were communicated in seminar lectures given by Prof. Belotserkovskii at several American universities during a 4-week visit in November - December, 1978. In response to numerous requests Prof. Belotserkovskii made available the manuscripts of two reports which describe in some detail the computational techniques employed in the numerical solutions of the problems surveyed in his seminar talks.

This report surveys results of research at the Computational Center of the USSR Academy of Sciences, Moscow, over the past decade in some problems of planar and three-dimensional transonic flows of a perfect gas. Although most of these results have previously appeared in various Soviet journals, this report nevertheless gives a coherent review of the advances in the computation of transonic flows at one of the foremost centers of the Soviet Union.

The hallmarks of their numerical techniques are that they are:

(1) typically differentially and globally conservative, and

(2) careful attention is made to minimize truncation errors while at the same time the favorable properties of the computational schemes are exploited, e.g., the effective viscosity of the finite-difference equations (to promote calculational stability) and (physically interpretted) the ability to compute the essential features of separated regions of recirculating flows (e.g., wakes) wholey within the framework of the Euler equations.

This work involves a careful and mutually beneficial blending of analysis and numerical computations to develop a complete picture of complex flows.

The numerical methods are illustrated by a great variety of computational results which are supported by analysis and compared with experimental results in some cases. Wherever possible English translations of the references have been cited.

The careful typing of the edited manuscript by Miss Vicki Brewer deserves a special note of appreciation. Finally, I am pleased to acknowledge Contract N00014-79-M-0022 from the U.S. Office of Naval Research which made possible the publication and distribution of this report.

W. L. Melnik, Editor

Professor, Aerospace Engineering Dept.
University of Maryland at College Park

TABLE OF CONTENTS

Chapter		Page
ABSTRACT		ii
PREFACE		iii
LIST OF FIGURES		vi
1.	INTRODUCTION	1
2.	HODOGRAPH PLANE	4
3.	MINIMUM DOMAIN OF INFLUENCE OF MIXED FLOW	8
	3.1 General Results	8
	3.2 Domains of Influence in Flow Around Bodies With a Detached Shock Wave	13
	3.3 Supersonic Flow Around Blunt Bodies With a Break in the Generator of the Contour	14
	3.4 Flow Around Blunt Bodies at Low Supersonic Velocities	18
4.	SECONDARY SHOCK WAVES	20
	4.1 Formation of a Shock Wave Within the Minimum-Domain of Influence	20
	4.2 Spoiling the Continuous Supersonic Flow Domain in the Characteristic Triangle Bounded by the Profile and the Adjoining M-Domain	21
	4.3 Formation of Imbedded Floating Shock Waves in Flows Past Profiles With a Corner	24
	4.4 Calculation of Floating and Secondary Shock Waves	26
5.	LOCAL SUPERSONIC ZONES	32
	5.1 "Large Particles" Method	32
	5.2 Calculation of Transonic and "Supercritical" Flows	37
6.	ON THE QUESTION OF EXTREMALITY OF THE ENTROPY ON THE STAGNATION STREAMLINE IN THREE-DIMENSIONAL FLOW	41
REFERENCES		43

LIST OF FIGURES

Figure		Page
1.	General features of the flow around a body with a detached bow shock	47
2.	Ratio of the shock curvature to its distance from the axis of symmetry at the sonic point as a function of the relative speed coefficient	47
3.	Multisheeted surface of the stream function in the hodograph plane	48
4.	Nature of the flow in the neighborhood of point K as a function of the parameter ω/A_2	48
5.	Classification of domains of influence of bluntness for two-dimensional and axisymmetric bodies	48
6.	Domains of influence in flow of a perfect gas (k = 1.4) around a circular cylinder: I for $M_\infty \leq 1.69$; II for $M_\infty > 1.69$	49
7.	Domains of influence in flows of a perfect gas (k = 1.4) around a sphere: II for $1.1 < M_\infty < M_2 = 3.7$; III for $3.15 \leq M_\infty < \infty$	49
8.	Computational mesh for Scheme I of the Method of Integral Relations	50
9.	Computational mesh for Scheme II of the Method of Integral Relations	50
10.	Geometry of supersonic flow with $M_\infty = 4$ past a spherically-capped reversed cone of $\chi = 30^0$ half-angle	50
11.	Geometry of flow around spherically-capped noses of reversed cones with $M_\infty = 10$ and $\chi = 33^0$ and $43^0 30'$	50
12.	Distribution of the normal, u_i, and tangential, v_i, velocity components across the shock layer of the bodies of Fig. 11, calculated from Scheme II	50

Figure		Page
13.	Computational mesh for Scheme III of the Method of Integral Relations	51
14.	Geometry of Detached Bow Shock in supersonic flow of a perfect gas (k = 1.4) past a sphere	51
15.	Comparison of numerical results with experiment (points) of Bedin and Mishin [30] for supersonic flow (k = 1.4) past a sphere	51
16.	Calculated surface pressure distribution along a sphere with k = 1.4	51
17.	Supersonic flow past various ellipsoids: Comparison of numerical results with experiment (points) of Maslennikov, et al [30] in (d) and of Riabinkov [17] in the remaining graphs	52
18.	Local supersonic "Zone I" in a subsonic potential flow according to Nikol'skii and Taganov [6]	52
19.	(a) Zone III in the physical plane	52
	(b) Mapping of Zone III in the hodograph plane	52
20.	The collapse of the continuous supersonic flow in the characteristic triangle Δ which adjoins the minimal domain of influence as the angle of the infinite blunted wedge increases	53
21.	Supersonic flow past a wedge-slab body with attached shock wave: AB, AC, AD - characteristics of the first family, BE of the second family	53
22.	Supersonic flow about truncated cones, $M_\infty = 100$, k = 1.4 and $\omega_0 = 54.5^0$: (a) $\omega_1 = 20$; (b) $\omega_1 = 10^0$; (c) $\omega_1 = 0^0$	54
23.	Two-dimensional ($\nu = 0$) and axisymmetric ($\nu = 1$) supersonic flow past a straight line profile with a circular nose and corner at $\chi = 68^0$	54

Figure Page

24. Surface pressure distribution along cones and wedges with various nose blunting 55

25. Surface pressure distribution over spherically blunted cylinders of various segment semi-angles χ having a sonic corner 55

26. Bow shock and imbedded floating shock for spherically blunted bodies with a sonic corner 55

27. Supersonic flow around spherically blunted cones with $M_\infty = 4$ and $k = 1.4$ 56

28. Effect of the corner point on the position of the limiting characteristic with $M_\infty = 4$; $k = 1.4$ and $\omega = 0^0$ 56

29. Coordinates of the shock waves on spherically blunted cones at $M_\infty = 6$ 56

30. Imbedded floating shock and surface pressure distribution over a double cone in supersonic flow, $M_\infty = 6$, $k = 1.4$ with $\alpha = 0^0$ and 5^0 57

31. Density profiles for boundary conditions of no-slip (— — — —) and vanishing of velocity component normal to surface (————) . 57

32. Lines of constant Mach number (isotachs) in supercritical flow ($M_\infty = 0.9$) around flat-faced cylinders of various lengths 57

33. Comparison of numerical results (————) with the asymptotic steady state [31,32] for sonic flow past a flat-faced cylinders 57

34. Isotachs in transonic flow around a two-dimensional 24 per cent circular arc profile; critical Mach number, $M_\infty^* = 0.65$ 58

35. Isotachs in transonic flow around a 24 per cent axisymmetic body (generated by revolution of a circular arc profile); critical Mach number, $M_\infty^* = 0.86$ 59

Figure | Page

36. Isotachs in transonic flow around a 12 per cent circular arc airfoil; calculated by the "large particles" method ———— , — — — experiment of Wood and Gooderum [39] 60

37. Isotachs in sonic flow past a space vehicle of the Apollo type. 60

38. Supersonic flow patterns around a short circular cylinder and a sphere 61

39. Isotachs in transonic flow around a sphere with upstream injection on the body axis, $\rho_c = 2.9$ and $M_c = 1.0$, i.e., $u_c = -1.0$, $v_c = 0$. 61

40. Special coordinate system generated by the stagnation streamline 41

1. INTRODUCTION

Much attention has recently been given to the investigation of transonic problems of gasdynamics. Such flows occur, for example, in nozzles, around a body with a detached bow shock, around convex corners, as well as on wings with imbedded local supersonic regions.

Difficulties arise in theoretical analysis of such problems primarily because of the fact that there is no complete mathematical formulation of the problem in a number of cases. In mixed flow domains complex phenomena occur: so-called secondary "suspended" compression shocks can originate behind the bow wave and for supercritical flight Mach number local supersonic domains can also be closed off by compression shocks. The mechanism by which such phenomena occur has not been sufficiently studied and questions regarding the region of influence and its adaptation to a change in flow parameters also remain open. Classical analytical methods, developed for plane potential flows, which predominantly utilize the hodograph plane, do not as a rule apply here. Numerical solutions of these problems involve many difficulties, and require the construction of special schemes for the integration of elliptic-hyperbolic equations.

If there is a break (corner) in the generator of a blunt body within the domain of influence of the flow, and the free stream is altered so that the local speed of sound occurs at this corner, then the analysis of such a flow is complicated substantially by the existence of this singularity. The flow expansion around the corner will be in the mixed transonic regime and is characterized by an abrupt change in both magnitude and direction of velocity. Moreover, a secondary compression shock can occur in the supersonic zone of this flow which substantially affects the whole flow pattern. It should also be noted that the computational results for the flow in the

domain of influence of the bluntness (M-domain) serve as the initial data for the calculation of the supersonic zone. Construction of the solutions in the transonic domain for a body with a corner must be made with special care since even slight inaccuracies in the calculations will not permit continuation of the computation into the supersonic domain.

A study of the flow properties around blunt bodies at low supersonic Mach number is of no less interest. As the free stream Mach number decreases, the domain of mixed flow influence increases. In examining such a problem it is necessary to take account of the transonic nature of the flow in the zone between the sonic line and the limiting characteristic separating the M-domain. Perturbations in the transonic domain affect the shape of the sonic line, and, therefore, the whole flow in the mixed zone. The solution of the boundary value problem becomes increasingly sensative to changes in initial data, so that round-off errors increase, and an instability in the computation is manifested. All this demands the construction of special numerical schemes. Consequently it is important to identify the existence of boundaries of distinct minimal domains of influence of the bluntness.

Only careful numerical experiments utilizing high-speed computers give quantitative data and a complete picture of the flow in such complex problems. An attempt is made to analyze and discuss some transonic flow properties (the solutions in the neighborhood of the sonic line, the formation of secondary compression shocks, the shape of the minimal domain of influence, etc.) from the aspect of analytical and numerical solutions.

It should be mentioned that precisely by numerical means are secondary compression shocks, non-monotone sonic lines, etc., successfully detected and constructed. At the same time, the conditions for spoiling the continuous solution, and the regularities associated with different kinds of domains

of influence, have been delineated analytically. In examining the flow around a corner, the effective construction of numerical schemes turned out to be possible only when utilizing asymptotic methods of solution of the differential equations. Therefore, the combination of both analysis and numerical solutions prove to be quite fruitful.

A number of papers have been devoted to the study of these questions. We consider in this report the results of investigations of the direct two-dimensional (planar or axisymmetric) problem obtained by using the methods of integral realtions [17,23,24,26,28,29,36] and "large particles" [31,32,37], which represents part of an ongoing research program in transonic flows.

2. HODOGRAPH PLANE

In analyzing plane stationary flows behind a shock it is convenient to use the gasdynamics equations written in a local streamline coordinate system:

$$(1 - M^2)\,\frac{\partial \ell n p}{\partial s_1} = kM^2\,\frac{\partial \beta}{\partial s_2}\,, \qquad \frac{\partial \ell n p}{\partial s_1} = -kM\,\frac{\partial \beta}{\partial s_1} \tag{1}$$

or in the form [1]

$$(M^2 - 1)\,\frac{\partial \ell n \lambda}{\partial s_1} = \frac{\partial \beta}{\partial s_2}\,, \qquad \frac{\partial \beta}{\partial s_1} = \frac{\partial \ell n \lambda}{\partial s_2} - \frac{1}{kM^2}\,\frac{d \ell n p_o}{d s_2} \tag{2}$$

Here λ is the velocity magnitude, made dimensionless by the maximum adiabatic velocity, M - the Mach number, β - the slope of the velocity vector measured counter-clockwise, p - the pressure, p_o - the total pressure, and k is the adiabatic index; $\partial/\partial s_1$, $\partial/\partial s_2$ - derivatives with respect to the directions of the velocity vector and its normal obtained by rotation of the velocity vector counter-clockwise through an angle $\pi/2$.

Equations (1) and (2) can be transformed (by using differential geometry formulas) into equations in a ϕ,Ψ coordinate system, where Ψ,ϕ are families of streamlines and their orthogonal trajectories since $h_1 \partial/\partial s_1 = \partial/\partial\phi$, $h_2 \partial/\partial s_2 = q\,\partial/\partial\Psi$; the Lame coefficients h_1, h_2 are given by the formulas [7]

$$h_1 \lambda \exp\left[-\frac{1}{k}\int \frac{d \ell n p_o}{M^2}\right] = \Phi(\phi), \qquad h_2 q(\lambda) = F(\Psi); \tag{3}$$

$$q(\lambda) = \lambda\left(\frac{k+1}{2} - \frac{k-1}{2}\,\lambda^2\right)^{1/(k-1)}.$$

Here $\Phi(\lambda)$, $F(\Psi)$ are arbitrary functions governing the numbering of the lines in the ϕ,Ψ families.

In the case of irrotational flows (for p_o = const), the Chaplygin equations can be obtained from the equations in ϕ,Ψ coordinates (by a change in the role of the dependent and independent variables).

Equations (3) permit the investigation of singularities of a mapping in the ϕ,Ψ plane. Indeed

$$\frac{\partial(\phi,\Psi)}{\partial(x,y)} = \frac{\partial(\phi,\Psi)}{\partial(s_1,s_2)} = \frac{1}{h_1 h_2} = \lambda q(\lambda)\exp\left[-\frac{1}{k}\int \frac{dp_o}{M^2}\right],$$

hence, for $0 < \lambda < (k+1)^{1/2}(k-1)^{-1/2}$ a mapping in the plane is locally one-to-one (x,y are Carteisan coordinates in the physical plane).

Let us consider the mapping of the velocity (λ,β) and pressure (p,β) in the hodograph plane; the former is more convenient for potential flow investigations, and the latter for rotational flow investigations.

It follows from the expressions for the Jacobians $J = \partial(p,\beta)/\partial(x,y)$, $I = \partial(\lambda,\beta)/\partial(x,y)$ of the transformations, using (1) and (2), that the mapping of subsonic domains in the $p\beta$ plane (and in the $\lambda\beta$ plane in the potential flow case) can only have isolated singularities [2,3]; however, this does not mean that the image of the subsonic domain in the $p\beta$ plane cannot be many sheeted (on the whole); the flow can only be single-valued in the physical plane.

A mapping of supersonic domains in the $p\beta$ plane can have folds; their edges (on which J changes sign) are called branch lines. A branch line can be a characteristic if J undergoes a discontinuity upon passing through it; in the general case a branch line is the envelope of characteristics of one family in the $p\beta$ plane, and the geometric locus of cusps of the second family of characteristics. A mapping of a rotational flow in the $\lambda\beta$ plane can have branch lines even in the subsonic domain. In the general case, a branch line of this mapping is a characteristic only in the potential flow case [3]. A classic illustration of the flow having a fold in the $\lambda\beta$ plane is a Laval nozzle; the branch lines are here characteristics issuing downstream from the center-line of the nozzle.

The edge of the fold of the inverse mapping is called a limit line. The presence of a limit line indicates that the flow whose image has been found in the hodograph plane can not be realized in the physical plane.

The characteristics equation in the pβ plane have the form:

$$\pm d\beta_{1,2} = -\frac{\sqrt{(M^2-1)}}{kM^2} d\ell np \quad . \tag{4}$$

Hence it follows that for $1 < M < \infty$ the first family characteristic always makes a negative angle with the p-axis, and a characteristic of the second family a positive angle; in some cases this permits establishment of the form of the branch line (if it exists).

The characteristics in the λβ plane are given by

$$\pm d\beta_{1,2} = -\sqrt{(M^2-1)}\, d\ell n\lambda - \frac{\sqrt{(M^2-1)}}{kM^2} d\ell np_o . \tag{4'}$$

which describe epicycloids in the case of potential flow ($d\ell np_o = 0$).

THEOREM 1. The image in the λβ plane of a segment of characteristic contained in the domain of monotonicity of the function $p_o(\Psi)$ will intersect an epicycloid of the same family not more than once. A segment of a characteristic of the first (second) family, drawn in the direction of diminishing total pressure from the point of intersection with the epicycloid of the same family, is located above (below) this epicycloid [4].

THEOREM 2. The image in the λβ plane of a characteristic drawn in the domain behind the shock located between two epicycloids of the same family which are separated by a distance (in the β direction) not exceeding

$$\frac{1}{k} \left| \ell n \frac{p_{omax}}{p_{omin}} \right| ,$$

where p_{omax} and p_{omin} are the maximum and minimum values of the total pressure behind the shock (depending on the free stream velocity) and k is the

adiabatic index.

THEOREM 3. If the velocity vector is continuous at some point in the physical plane, then the characteristic at the corresponding point in the $p\beta$ plane is either a smooth curve, or has a cusp (the latter can be realized only in the case when intersection with a branch line occurs at this point). This property of the characteristics in the $\lambda\beta$ plane only exist under the additional condition of continuous differentiability of the total pressure and the velocity vector at the corresponding point of the physical plane.

3. MINIMUM DOMAIN OF INFLUENCE OF MIXED FLOW

The minimum domain of influence of mixed sub- and supersonic flow (the M-domain) is characterized by the fact that small perturbations of its boundaries are propagated throughout this domain. In the general case the M-domain boundary is delineated by segments of the body-profile which may include a tangential discontinuity (corner), the axis of symmetry, the bow shock, the limiting characteristic, and the sonic line.

3.1 GENERAL RESULTS

In order to establish the location of the M-domain in the hodograph plane, it is necessary to know the sign of the Jacobian of the mapping at points of the boundary.

THEOREM 4. The following inequalities hold:

1. On a straight-line wall

$$I = \partial(\lambda,\beta)/\partial(x,y) \gtrless 0,\quad I = \partial(\lambda,\beta)/\partial(x,y) \gtrless 0 \text{ for } \lambda \gtrless 1 ;$$

2. On a free boundary $J \geq 0$

3. On the shock polar $J \geq 0$, $I \lesseqgtr 0$ for $M \lesseqgtr A(M_\infty k)$,

where M_∞ is the free-stream Mach number, and A is some constant; $A \gtrless 1$ for $M_\infty \gtrless M_0(k)$, where $M_0(k)$ is some constant.

THEOREM 5. The image of a convex corner in the $p\beta$ and $\lambda\beta$ planes is mapped by a characteristic of the potential flow which has no turning points*.

THEOREM 6. In potential flow, the image in the $\lambda\beta$ plane of the neigh-

---

* This is proved in [5] for potential flow.

borhood of a convex corner covered by characteristics emerging from this point is located on one side of the epicycloid mapping the corner.

Let K denote a point of the sonic line at which it is convex relative to the lines ϕ = constant (sonic line at the point K_+ turns the convexity towards the supersonic velocity region, and at K_- towards the subsonic domain). Let L denote a point of the sonic line at which the sign of the streamline curvature changes during passage through it. If the vorticity is zero at the point K, then it coincides with L.

THEOREM 7. There are no points K_- located within the potential flow domain.

THEOREM 8. If there is displacement along the sonic line in potential flow so that the subsonic domain lies on the left, the velocity vector will be rotated monotonely clockwise [6].

THEOREM 9. The slope of the velocity vector β changes monotonely with displacement along a sonic line segment in a rotational flow which does not contain the points K or L. A change in the direction of variation of β occurs at each of the points K or L [7].

Thus, branch lines of the mapping in the $\lambda\beta$ plane (an odd number at each of the points) pass through the points K and L.

THEOREM 10. If the acceleration of the flow at the sonic line is bounded, then $\partial(p,\beta)/\partial(x,y) = 0$ at the point L.

Let γ denote the angle through which it is necessary to turn the tangent to the sonic line counter-clockwise (at the sonic point of the shock) so that it would coincide with the velocity vector.

THEOREM 11. If the curvature of the shock wave at the sonic point does not vanish or become infinite, then $\gamma > \frac{1}{2}\pi$ for $M_\infty < M_0(k)$ and

$\gamma < \frac{1}{2}\pi$ for $M_\infty > M_0(k)$ [8].

The constant $M_0(k)$ is here the same as in THEOREM 4 (see Fig. 1 and 2).

Theorem 11 can be generalized partially to the case of axisymmetric flow. Let σ denote the slope of the shock to the free stream velocity vector measured counter-clockwise.

THEOREM 12. If the curvature of the shockwave at the sonic point of an axisymmetric flow does not become zero or infinite, then the following inequalities hold:

1. $\gamma < \frac{1}{2}\pi$ for $\sigma < 0 < \frac{1}{2}\pi$ and $M_\infty > M_0(k)$.
2. $\gamma > \frac{1}{2}\pi$ for $-\frac{1}{2}\pi < \sigma < 0$ and $M_\infty < M_0(k)$.

In the remaining cases the angle γ (Fig. 2) depends on the shock curvature, the distance from the axis of symmetry, and the free stream velocity [9].

Let δ denote the angle between the sonic line and the profile on the downstream side of the sonic line.

THEOREM 13. If the vorticity is zero along the contour of a smooth profile, then $0 < \delta < \frac{1}{2}\pi$ on the convex profile, and $\frac{1}{2}\pi < \delta < \pi$ on the concave profile (if the acceleration $\partial\lambda/\partial s_1$ does not vanish or become infinite at the sonic point of the profile) [8].

The next theorem follows from 11 and 13.

THEOREM 14. If the assumptions of Theorems 11 and 13 are satisfied, in the case of symmetric flow around a smooth convex profile with a detached shock an odd number of points K exists on the sonic line for $M_\infty > M_0(k)$ (at least one point K_+); for $M_\infty < M_0(k)$ the number of points K is zero or even (the number of points K_+ equals the number of points K_-) [8].

THEOREM 15. At a convex corner of the profile, the sonic line is orthogonal to the "subsonic" direction of the angle (in transonic flow).

This property has been proved in [10] for potential flow.

The theorems considered above assist in classifying the minimum domains of influence for an unbounded flow around a profile (or axisymmetric body) and are in good agreement with results of calculations.

THEOREM 16. In symmetric flow around a smooth convex profile (if the assumptions of Theorems 11 and 13 are satisfied), the number of branch lines of a mapping in the $\lambda\beta$ plane which intersect the sonic line is zero or is even if $M_\infty < M_0(k)$; the number of these branch lines is odd if $M_\infty > M_0(k)$ [7].

The following theorems characterize the flow in the neighborhood of the point K of the sonic line.

THEOREM 17. If a point K exists on the sonic line, at which the flow acceleration does not become zero or infinite, then the following inequalities are satisfied [7]:

$$\left(\frac{\partial\lambda}{\partial s_1}\right)^2 \gtrless \frac{1}{Rk(k+1)}\,\frac{d^2s}{d\psi^2} - \frac{1}{R^2k^2(k+1)}\left(\frac{ds}{d\phi}\right)^2$$

at the point K_+ or K_-. Here R is the gas constant, and s the entropy.

Let AK_+B denote the line formed by the characteristics issuing downstream from the point K_+ (we consider the direction "downstream" to be along the streamlines from the subsonic domains).

THEOREM 18. At least one branch line of the mapping in the $\lambda\beta$ plane which passes through the point K_+ in the supersonic domain will be downstream of the line AK_+B [7].

If the flow acceleration at the point K does not become zero or infinite, the flow in the neighborhood of this point can be investigated analytically [11]. Equations of transonic rotational flow are derived by the small parameter method

$$u\frac{\partial u}{\partial \phi^0} - \frac{\partial v}{\partial \phi^0} = 0\,, \quad \frac{\partial v}{\partial \phi^0} + \frac{\partial u}{\partial \Psi^0} = \omega\Psi^0\,,$$

$$\omega = (k+1)(W_1 - W_0^2)\,,\ W_0 = \frac{1}{kR}\frac{ds}{d\Psi}\bigg|_K\,,\ W_1 = \frac{1}{kR}\frac{d^2s}{d\Psi^2}\bigg|_K\,, \tag{5}$$

$$\lambda = 1 - \frac{u(\phi,\Psi)}{k+1} = 1 - \varepsilon^2\frac{u(\phi^0,\Psi^0)}{k+1}\,,$$

$$\beta = \frac{v(\phi,\Psi)}{k+1} = s_1^2\phi^0 W_0 - \varepsilon^3\frac{W(\phi^0,\Psi^0)}{k+1}\,,\ \phi = \varepsilon^2\Psi^0,\ \Psi = \varepsilon\Psi^0\,.$$

Here ε is a small parameter characterizing the size of the neighborhood of the point K.

The equations obtained have an exact solution, analogous to the exact solution of the transonic potential flow equations, which was used in [12] to investigate the flow in the neighborhood of the center line of a Laval nozzle under the condition that the acceleration does not become zero or infinite.

This solution has the form:

$$u = A\phi - \frac{A^2-\omega}{2}\phi^2,\quad v = (k+1)W_{0\phi} + A^2\phi\Psi - \frac{A(A^2-\omega)}{6}\Psi^3\,,$$

$$A = -(k+1)\frac{\partial\lambda}{\partial s_1}\bigg|_K$$

The solution so obtained can be analyzed. For example, a three--valued mapping function can be constructed in the hodograph plane; the geometry of the branch line is studied as a function of the parameter ω, which characterizes the velocity (Fig. 3). Also the characteristics

pattern (Fig. 4) is of considerable interest, particularly, when $\omega > A^2$ (the point K_-). Analogous investigations have been made in [13,14] for axisymmetric and three-dimensional rotational flows.

3.2 DOMAINS OF INFLUENCE IN FLOW AROUND BODIES WITH A DETACHED SHOCK WAVE

Let us examine the boundaries of various kinds of minimal domains of influence in the flow around smooth plane or axisymmetric bodies with a detached shock. A schematic diagram of the domains of influence realized for such flows in given in Fig. 5 (the velocity vector at the point K is orthogonal to the sonic line).

The essential characteristics of each type of domain of influence are the slope of the sonic line to the velocity vector on the shock (γ) and on the body (δ). The minimum domain of influence shown in Fig. 5. holds for the following combinations of values of these angles [8,9,17]:

1st type : γ oblique , δ acute;

2nd type : γ acute , δ acute;

3rd type : γ acute , δ oblique.

Since the angle δ is always acute in the plane case ($\nu = 0$) in the flow around a convex profile (Theorem 13), the third type of domain of influence is not realized. The transition from the first into the second type occurs for $M_\infty = M_0(k)$ (Theorem 11). The graph of $M_0(k)$ is given in Fig. 2, where $M_0 = 1.6358, 1.6895$ and 1.7421 for $k = 1.2, 1.4$, and 1.6 respectively. Flow patterns and domains of influence for $M_\infty = 1, 1.5, 3, 3.10$ ($k = 1.4$, circular cylinder), obtained from numerical calculations, are presented in Fig. 6 [8,17,29].

The situation is more complicated in the axisymmetric case ($\nu=1$). According to Theorem 12, the angle γ is acute for $M_\infty > M_0(k)$. Therefore,

even in the axisymmetric case the first type of domain of influence (if it exists) can hold only for $M_\infty < M_0(k)$, when the angle γ will be oblique, which governs the location of the sonic point of the shock wave with coordinates R/y, M_∞ (R is the radius of curvature of the shock) relative to the dividing curve $f(M_\infty,k)$, on which $\gamma = \frac{1}{2}\pi$ [9] (Fig. 2).

It is interesting to note that domains of influence of the second type ($\gamma < \pi/2$) were realized in computations of the flow around a sphere (k = 1.4, $M_0(k)$ = 1.69) down to M_∞ = 1.1. The magnitude of the angle δ varied thus in this case: $\delta = \pi/2$ for $M_\infty = M_2 = 3.7$ (the point K is on the body); for $M_\infty < M_2$ the angle δ is acute (domain of influence of the second type); for $M_\infty > M_2$ the angle δ is oblique (domain of influence of the third type).

Flow patterns and domains of influence for a sphere (k=1.4, and M_∞ = 1.15, 1.5, 2,3,4), obtained from numerical computations, are presented in Fig. 7 [17,28].

3.3 SUPERSONIC FLOW AROUND BLUNT BODIES WITH A BREAK IN THE GENERATOR OF THE CONTOUR

Supersonic flow around blunt bodies which have a corner are calculated by scheme I or II of the Dorodnitsyn-Belotserkovskii method of integral relations [8,17,23,24,26] whose computational meshes are shown in Fig. 8 and 9.

The first scheme of the integral relations method is applied in both the domain up to the corner and in the supersonic expansion around it, where the governing equations are written in a polar coordinate system centered at the corner. The resulting system of ordinary differential equations is integrated numerically along the shock layer starting from the axis of symmetry. In the neighborhood of the corner, where the Prandtl -Meyer solution

holds, a differential relation is used which is the compatibility condition along the second family of characteristics [17].

In the second scheme of the method (Fig. 9), the domain of influence of the bluntness is delineated exactly because of the simultaneous construction of the limiting characteristic, which substantially increases the accuracy of the calculation in each approximation. Here the asymptotic Vaglio-Laurin-Shugaev solution, reduced to a form convenient for calculations [17,25,26], is utilized in the neighborhood of the corner (the domain G).

The solution which describes plane and axisymmetric transonic flow of a perfect gas in the neighborhood G of a corner has the form of a power series in the distance n_o from the body surface ($n_o = 0$) with coefficients dependent on the corresponding self-similar variable ζ:

$$u = 1 + (k+1)^{-1/3} \sum_{i=0}^{\infty} u_i(\zeta) n_o^{(2+i)/4}, \quad v = \sum_{i=0}^{\infty} v_i(\zeta) n_o^{(3+i)/4},$$

$$\zeta = (k+1)^{-1/3} s_o n_o^{-5/4}, \qquad n_o = n/r_o^*, \qquad (6)$$

$$s_o = (s-s^*)/r_o^*,$$

where u, v are velocity components (referred to the critical speed of sound) along the tangent and normal to the body surface in the subsonic neighborhood of the corner; quantities at the sonic point on the body are denoted with an asterisk (Fig. 8). The main term of this expansion described two-dimensional transonic potential flow in the neighborhood of the corner (primes denote derivatives with respect to ζ):

$$u_o = g', \quad v_o = (7g - 5\zeta g')/4$$

where

$$g'' = B_1(21g - 25\zeta g')/16, \quad B_1^{-1} = g' - (25\zeta^2)/16.$$

It is interesting to note that the function $g(\zeta)$, corresponding to the potential of this flow, can be expressed in the parametric form [27]:

$$g = (25/42)5^{-1/8}(5Z^2+5Z-4)(1-Z)^{-7/8}(1+3Z/5)^{-9/8}C^{-3} ,$$
$$\zeta = -2.5^{-3/8}Z(1-Z)^{-5/8}(1+3Z/5)^{-3/8}C^{-1}, \quad -5/3 < Z < 1 . \qquad (7)$$

If the scale factor C=1, then $g'(1)=0$, where $g \simeq (125/56)2^{-1/5}(-\zeta)^{7/5}$ as $\xi \to \infty$ and $g \simeq \zeta^3/3 - 675/96\ 10^{-1/3}\xi^{1/3}$ as $\zeta \to \infty$ (refer to equation (8) below, for the relationship between ξ and Z).

The terms of the expansion (6) of a higher order of smallness, which take into account the rotational and axisymmetric nature of the flow (u_i, v_i, i = 1,2,...), are found from the solution of linear non-homogeneous ordinary differential equations. The functions u_i, v_i must satisfy the boundary conditions in both the subsonic domain (zero normal component of velocity relative to the body on its surface) and in the supersonic domain where the solution describes a flow of Prandtl-Meyer type.

An analytic solution of this system was found in [17,26] by F.V. Shugaev. Let us represent the quantities u_i, v_i as the sum of the particular solution $u_i^{(1)}, v_i^{(1)}$ of the non-homogeneous system, and the general solution $u_i^{(2)}$, $v_i^{(2)}$ of the homogeneous system. If $\Phi_i(\zeta)$ is introduced, so that the solution $u_i^{(2)}, v_i^{(2)}$ of the corresponding homogeneous system would be written as

$$u_i^{(2)} = \frac{d\Phi_i}{d\zeta} , \quad v_i^{(2)} = \frac{7+i}{4}\Phi_i - \frac{5}{4}\zeta\frac{d\Phi_i}{d\zeta} ,$$

then a second order equation is obtained to determine Φ_i

$$(16g'-25\zeta^2)\Phi_i'' + [16g'' + 5(5-2i)\zeta]\Phi_i' - (7+i)(3-i)\Phi_i = 0$$

Utilizing the parametric representation (7) of the function $g(\zeta)$ and making the change of variables

$$t_i = \Phi_i(1-Z)^{(7+i)/8}(1+\frac{3}{5}Z)^{3(7+i)/8}, \quad \xi = \frac{1}{4}[2 - \sqrt{(3/2(1-Z))}] \qquad (8)$$

we obtain the hypergeometric equation

$$6\xi(1-\xi)t_i'' + (9+2i)(1-2\xi)t_i' - 2(7+i)(9+i)t_i = 0$$

Its solution is made up of Jacobi polynomials

$$t_i = [\xi(1-\xi)]^{(5/2+i/3)} \frac{d^{(7+i)}}{d\xi^{(7+i)}} \{[(1-\xi)]^{(2i/3+9/2)}\},$$

which permit expression of the quantities u_i, v_i in finite form.

Such a representation turns out to be quite convenient for calculations in the G-domain since direct integration of the original system would give rise to definite difficulties. Computations have shown that it is sufficient to use the first two or three terms of the solution (6)-(8) to construct the flow in the neighborhood of an angular point; the influence of the remaining terms is negligible.

Because the limiting characteristic of the domain of influence of the bluntness approaches the corner from the supersonic side, expansion (6), which is valid only near the sonic line in the supersonic domain, turns out to be inadequate. Hence, it is necessary to continue the solution into the purely supersonic domain, which has indeed been found as a correction in powers of r_1 (Fig. 8) of the type $\Sigma f_i r_1^{\alpha_j}$ to the fundamental Prandtl-Meyer solution.

The customary algorithm of scheme II is applied outside the domain G. Systems of ordinary differential equations are integrated across the shock layer between the bow shock wave and the body, while the additional conditions of "joining" both solutions along the boundary of this domain make the problem single-valued.

On the whole we have succeeded in obtaining algorithms which enable us to compute solutions with a high degree of accuracy. The solution outside the zone of influence of the bluntness is constructed by the usual method of characteristics. Some results of computations obtained by A. Bulekvaev, E.S. Sedova and F.V. Shugaev [17,26] are presented in Figs.10-12.

The geometry of the detached bow shock, sonic line and limiting

characteristic for perfect gas flow (k=1.4, M_∞=4) around a spherical segment with a sonic corner followed by a reversed cone of $\chi=30^0$ half angle, are shown in Fig. 10; the corresponding features are shown in Fig. 11 for $\chi=33^0$ and $43^030'$ with M_∞ = 10. The variation of the velocity components (along n,s, respectively) on the axis of symmetry (i=0), the limiting characteristic (i=1), and the intermediate line (i=2) is given in Fig. 12. It is seen that the behavior of u_1 on the limiting characteristic depends strongly on the half-angle of the afterbody.

3.4 FLOW AROUND BLUNT BODIES AT LOW SUPERSONIC VELOCITIES

As has already been remarked, the construction of special numerical schemes would be required for the computation of mixed gas flows at low supersonic velocities. In this case, scheme III of the method of integral relations [17,24,28] turned out to be the most effective, wherein a representation of functions in two directions is used, and the original equations are approximated by a nonlinear system of algebraic equations in a curvilinear computational mesh Fig. 13.

With these schemes F.D. Popov [17] carried out calculations for free stream Mach numbers down to M_∞ = 1.05 for the complete set of gasdynamics equations which included effects of vorticity. The calculation of sonic flows (M_∞ = 1, potential flow), where the shock stands off at an infinite distance, was also carried out by the method of integral relations by P.I. Chushkin [29]. The results of some of these calculations are illustrated in Figs. 14-17. The geometries of the detached bow shock and limiting characteristic for flow of a perfect gas (k=1.40) past a sphere are shown in Fig. 14 and 15 for different M_∞. Experimental results of D.P. Bedin and G.I. Mishin are indicated by the open circles. Fig. 16 shows the pressure

distribution along the surface of a sphere (referred to the stagnation point pressure) for different M_∞. As the Mach number decreases, the pressure distribution differs more and more radically from the Newtonian distribution often utilized in the approximate theory of supersonic flow.

In Fig. 17d computational results (solid line) are compared with the experiments of V.G. Maslennikov et al. [30] for the bow shock standoff distance ε_0 along the axis of symmetry of a sphere as a function of the free-stream Mach number.

G.M. Raibinkov made a detailed experimental investigation of the flow behind a detached shock and presented the results in the form of tables and graphs [17]. Figure 17 (a,b,c,e,f) give a comparison between the experimental data of G.M. Riabinkov and the results of calculations by the method of integral relations for a sphere (δ=1) and ellipsoids of revolution (δ=0.5 and 2 where δ is the ratio between the vertical and horizontal axes of the ellipsoid). The pressure distribution along the body, as well as the shape and location of the bow shocks, are presented. It is seen that agreement between theoretical and experimental results is very good everywhere.

4. SECONDARY SHOCK WAVES

4.1 FORMATION OF A SHOCK WAVE WITHIN THE MINIMUM-DOMAIN OF INFLUENCE

It has been shown in [6] that potential flow in a local supersonic zone of definite type ("zone I") is spoiled if an arbitrarily small length of the profile segment bounding this zone becomes a straight line. Zone I is characterized by the fact that both characteristics go from each point of the profile segment bounding it to the sonic line (see Fig. 18).

It turns out that an analogous result holds even in the case of symmetric rotational flow around a smooth convex profile with a detached shock [4]. The existence of zone I here follows from Theorem 13 (Figs. 1, 19). Let us designate zone III as a subsonic domain of monotonely decreasing dependence of the entropy on the stream function. In the case of a strictly convex profile, there exists an ε-neighborhood of the sonic point of the profile, whose mapping in the hodograph plane is single-valued.

THEOREM 19. A profile segment bounding an ε-neighborhood of the sonic point of the profile in zone III, whose mapping is single-valued in the hodograph plane, cannot contain a straight-line section [4].

Therefore, making some part of the profile in the ε-neighborhood (for $\lambda > 1$) into a straight line results, independently of its length, either in such a deformation of the sonic line or the characteristics so that zone III will not contain the straight line section, or in the formation of branch lines which violate the one-sheetedness of the mapping of the orignal ε-neighborhood, or in the formation of a shock wave. Apparently, the first does not hold, since otherwise the solution of direct flow problem would not be unique or there would not be a continuous dependence on the boundary conditions. For the direct flow problem it can be shown that violation of the

one-sheetedness of the mapping is also impossible because in this case changes would occur in the flow which depend not on the length of the rectified section, but only on its location (under the condition that the flow in zone III remains continuous). *These considerations lead to the following* theorem.

THEOREM 20. If the problem of external flow around a profile with a detached shock is correct, then its solution is not generally continuous (in the domain behind the detached shock [4]).

4.2 SPOILING THE CONTINUOUS SUPERSONIC FLOW DOMAIN IN THE CHARACTERISTIC TRIANGLE BOUNDED BY THE PROFILE AND THE AJOINING M-DOMAIN

We assume the existence of a smooth convex profile such that the flow in the region behind the shock is continuous, and the entropy in the M-domain monotonely decreases with the stream function (i.e., the shock has turned the convexity towards the free stream). It follows from Theorem 13 that the boundary of the M-domain contains a segment of a characteristic of the first family AB, which has one end on the profile, and the other on the sonic line (Fig. 20).

Let Δ denote the triangle bounded by a characteristic of the first family AB, a characteristic of the second family AC, and the profile segment BC. The triangle Δ adjoins the M-domain from downstream (see Fig. 20).

THEOREM 21. Suppose part of a profile downstream of some point E is replaced by a straight line tangent to this point, and then consider upstream displacement of the point E. Before the point E enters into the M-domain *the continuous supersonic flow in the triangle* Δ collapses: either a secondary shock wave or a local subsonic zone arises in the flow [15].

In flow about a semi-infinite blunt wedge with a detached shock wave, either an imbedded shock or a local subsonic zone of isentropically retarded gas (Fig. 20) will arise as the vertex angle is gradually increased so long as the flow far downstream of the bow shock remains supersonic. An analogous result is obtained in the case of flow about a profile with a corner from which a sonic line originates.

We shall restrict the proof of the preceding theorem to the case of a smooth convex profile in incident flows with $M_\infty < M_0(k)$ (Fig. 20). In this case the first type of minimal region of influence of the blunt nose is found, bounded in the shock layer by the characteristic of the first family AB.

Integrating the compatibility relations on the characteristics in the direction of increasing entropy from point A to the profile contour, we obtain [15]

$$\begin{aligned} \beta_B &\geq \beta_A + I_1 = \beta_A + \frac{1}{2Rk} \int_{(AB)} \sin 2\alpha \, ds , \\ \beta_C &\leq \beta_A - I_2 = \beta_A - \frac{1}{2Rk} \int_{(AB)} \sin 2\alpha \, ds , \end{aligned} \tag{9}$$

where α = arc sin (1/M), β is the angle of inclination of the velocity vector to the axis of symmetry and R is the gas constant. Since both integrals are positive there must exist a point D on the profile contour, lying between points A and C in which $\beta_D = \beta_A$.

We subject the profile to a continuous deformation, replacing part of its contour located downstream from some point E, by the tangent to the contour at this point and then displacing the point E upstream from its aft-most

position all the way up to the point D. We shall show that just as soon as point E coincides with point D, either one of the aforementioned assumptions is contradicted or the minimal region of influence is reconstructed. Indeed,

$$\frac{1}{2Rk} \inf_{E\in[DF]} \int_{(AC)} \sin 2\alpha \, ds = \frac{1}{2Rk} \inf_{E\in[DC]} \int_{(AC)} \sin 2\alpha \, ds \geq \frac{1}{2Rk} \int_{(AP)} \sin 2\alpha \, ds$$

where P is the point of intersection of characteristics of the second family AC with characteristics of the first family DP.

Let us now define the point G on the original profile by the equality

$$\beta_G = \beta_D - \varepsilon .$$

In view of the convexity of the profile, point G lies between points D and C. If point E is located between points D and G, i.e., if

$$\beta_D \geq \beta_E > \beta_G$$

then we obtain

$$\beta_C = \beta_E > \beta_G = \beta_D - \varepsilon = \beta_A - \frac{1}{2Rk} \inf_{E\in[DC]} \int_{(AC)} \sin 2\alpha \, ds \quad ,$$

i.e., $\beta_C > \beta_A - I$, which contradicts the second of the inequalities (9).

Thus, while the problem of determining supersonic continuous flow in the characteristic triangle ABC from Cauchy data on the characteristic AB and the impenetrability conditions on the original profile BC had a solution in the large, this is no longer true for the profile deformed in the manner indicated.

In an analogous way the case $M_\infty > M_0(k)$ can be examined, as can the case in which the sonic line eminates from the corner on the profile. Results of numerical computations agree very well with the results of the analytical studies cited in this section for smooth bodies.

4.3 FORMATION OF IMBEDDED FLOATING SHOCK WAVES IN FLOWS PAST PROFILES WITH A CORNER

Let us now examine [33] the flow about a profile with a convex corner immersed in a uniform supersonic stream, especially when changes in entropy on the shock wave can be neglected. We shall also take advantage of the transonic approximation to the shock polar and the characteristics intersecting it.

First consider supersonic flow past a wedge-slab body (a profile with straight-line segments OA and AF in Fig. 21) with an attached shock wave. In Fig. 21a, OB is the straight-line segment of the shock wave; AB, AD, AC are the straight-line segments of characteristics of the first family while BE is a characteristic of the second family. The region behind the shock wave in physical space is mapped onto the velocity hodograph plane η,β where $\eta=(k+1)^{1/3}(\lambda-1)$, λ is the velocity coefficient, β is the angle of inclination of the velocity vector to the axis of symmetry, k is the adiabatic index; the axes β,y are directed vertically upward, the axes λ,x horizontally to the to the right. The mapping of the region OBEAO (Fig. 21b) is the segment of the characteristic $\overline{a_1a_2}$ of the second family $\beta = C - (2/3)\eta^{3/2}$; the point a_1 with coordinate β_1 lies on the shock polar $\beta=\Omega^{-1/2}(\eta_\infty-\eta)^{1/2}(\eta_\infty-\eta)$, the point a_2 lies on the η axis. The equations of the characteristics and shock polar are given in the transonic approximation.

Theorem 22. If the flow field about a profile with straight line segments OA and AF behind an attached shock wave is everywhere supersonic, then it cannot be continuous.

Let us examine the fan of characteristics of the first family emanating from the corner point A (subsequently denoted as fan A) in the physical plane (Fig. 21a). If the flow behind the shock wave is everywhere supersonic and

continuous, then every characteristic of the fan either intersects the shock wave or extends out to infinity. Corresponding to this, in the $\eta\beta$ plane, each characteristic of the first family passing through the characteristic a_1a_2 must end up either somewhere on the shock polar or at the point n, which also lies on the shock polar and represents the mapping of the uniform rectilinear flow at infinity. This represents a contradiction inasmuch as characteristics of the first family emanating from points of the segment ca_2 in the $\eta\beta$ plane cannot end up on the shock polar; consequently, if the flow is to be supersonic a secondary shock must arise.

This theorem with appropriate changes in formulation can also be extended to the case of a detached shock wave.

It can be shown [33], that the beginning of the shock does not lie at the apex of the convex angle, but again in the region covered by the characteristics of the fan A. The imbedded floating shock is inclined downstream from its origin. The end of the shock of the first family (where it degenerates into a characteristic) lies at an infinite distance from the profile. If a shock of the first family intersects the main shock wave or another shock, then at the point of intersection its intensity does not vanish.

The proof of these properties for IFS* is based on the one-to-one property of the mapping in the hodograph plane of the apex of the convex angle and its neighborhood covered by characteristics of the fan A.

We denote by Q_R the region bounded by the shock wave, the segment of profile OA, the imbedded floating shock, and the last characteristic of the fan A. In accordance with theorems of [33], the beginning of the shock lies either on this characteristic or on a characteristic of the first family located downstream of it. A study of the mapping of the region Q_R in the

---

* IFS - Imbedded Floating Shocks.

hodograph plane leads to the conclusion that the flow in the region Q_R does not depend on the shape of the profile over the segment AF. This feature was also observed in the numerical solutions of [17]. In the flow about a profile with a straight-line segment AF the last characteristic of fan A represents a branch line.

Finally, the following theorem can be established:

THEOREM 23. In the flow about a profile with a straight-line segment AF with $\beta_0 = 0$ the imbedded shock does not intersect the bow shock wave at a finite distance; apart from that, there are no other imbedded floating shocks of the first family.

In case there exists a second shock in flow about a profile with an afterbody segment AF having $\beta_0 > 0$, it must intersect the bow shock wave. Up to their point of intersection behind the bow shock wave, $\beta < \beta_0$. The bow shock wave after the point of intersection with a second shock (or the point of intersection with the last characteristic of the fan A, if there is no second shock) consists of an infinite number of segments with curvatures of opposite signs*; the oscillations in the angle of inclination of the shock wave decay with increasing distance from the profile. This result also agrees well with numerical results for bodies with corners [17,26].

4.4 CALCULATION OF FLOATING AND SECONDARY SHOCK WAVES

Imbedded "floating" compression shocks are formed behind the bow shock in the calculation of supersonic flow around blunt wedges and cones (smooth,

---

* The property of oscillation of the angle of inclination of the bow shock is found in connection with the theory of propagation of disturbances in the case of flow about wedge-shaped profiles.

with a break in the generator) in definite flow regimes [16,17]. These results demonstrate that effects due to viscosity (i.e., boundary layer separation) do not underlie such phenomenon (confirmed by experiment). In certain regimes of supersonic flow about blunt bodies (cones, wedges, etc.) imbedded floating shocks (IFS) arise in the flow field behind the bow shock which have a significant effect on their aerodynamic characteristics. This phenomenon was also noted earlier in experiments; its cause, however, was not particularly well understood. It was suggested by M.J. Lighthill, for example, that the shock was generated as the result of separation and subsequent reattachment of the boundary layer in the vicinity of the corner [33]. The reasons for the generation of IFS, the conditions under which they arise (body configuration, flight regime, etc.), and the properties of such flows have not been adequately studied to the present time.

We present here certain results of computations related to the generation of IFS. The computations were carried out by the aforementioned methods within the context of an ideal gas for both smooth blunt bodies and profiles with a sonic or supersonic corner [17].

Let us first consider those properties which lead to the generation of IFS. In flow about blunt cones or wedges there occurs a rapid deceleration of the flow in passing from the blunt nose portion to the straight portion of the contour. This results in crowding together of the characteristics and in the appearance of compression waves emanating from the body surface behind the corner. In those cases when the pressure gradient downstream from the characteristic bounding the region of influence of the blunt nose is large and the shock layer is sufficiently thick the compression waves coalesce into a shock wave of initially zero intensity which arises in the

interior of the flow.

An imbedded floating shock by analogy with characteristics, will be identified as a shock of the first (second) family if the tangent to it is achieved by rotating the velocity vector through a positive (negative) acute angle. Shocks of different families do not connect smoothly with each other.

Every instance of spontaneous generation of shock waves is always associated with the intersection of characteristics of one family. In such flows there arises an entire region doubly covered by characteristics of one family. Furthermore, the cusp of the envelope of these characteristics marks the beginning of the shock wave. The cusp itself does not yet belong to the discontinuity. The derivatives of velocity, density, pressure, etc., become infinite at the cusp, and hence the intensity of the IFS at this point must be zero and a "real" shock wave arises only subsequently.

In practice it is usually not necessary to determine exactly the point at which the envelope has a cusp or to start out the IFS at zero intensity. The shock wave is considered instead to emanate from the point of intersection of those characteristics of one family which are followed in the computations. It should be noted that IFS, in view of their relativity weak intensity, can be rigorously constructed numerically only by direct application of the method of characteristics.

Fig. 22, taken from [34], shows examples of numerical results for flow of an ideal gas (k=1.4) at M_∞ = 100 past a nose cone of semi vertex angle $\omega_0 = 54.5^0$ with conical afterbodies of various half angles $\omega_1 = 0^0, 10^0$ and 20^0. The generator of the body of revolution is described by the cross-hatched line ACB; AD represents the bow shock wave and BD, the characteristic of the second family along which characteristics of the first family intersect up

to point H (if such exists) denoted by a dot. In Fig. 22c the line CH is the last characteristic of the fan emanating from point C. The dot-dash line in Figs. 22a and 22b represents the pressure on pointed cones with semi apex angles of 20^0 and 10^0, respectively, for the same Mach number, M_∞. Lengths are referred to the radius of the cone at the corner and the surface pressures is divided by the stagnation pressure.

As indicated by the pressure distributions, in the third case, the IFS is generated inside the flow field, in the second, immediately behind the bow shock wave, and in the first case there is no IFS in the shock layer. Furthermore, it should be noted that as the angle of the conical afterbody ω_1 is decreased, there is a corresponding increase in the pressure gradient at the corner, and the shock layer becomes relatively thicker.

The calculations were obtained by the method of characteristics for an ideal gas; the initial conditions for the calculations were obtained from the exact solution for a pointed cone, insuring a high degree of accuracy in the computations. These examples show that the generation of IFS is not dependent on flow properties related to viscosity (i.e., separation of the boundary layer) and moreover that their occurrance is not related to the use of "coarse" initial data for the numerical calculation of the supersonic region by the method of characteristics.

Thus the regimes of flow about blunt cones and wedges which are conducive to the development of a positive pressure gradient behind the corner and a sufficiently thick shock layer lead to the generation of IFS, the position of which is determined by the intersection of two neighboring characteristics of the same (first) family.

We shall now consider several more examples. Shock waves (Fig. 23a) and surface pressure distributions (Fig. 23b) are shown for plane (ν=0) and

axisymmetric (ν=1) bodies described by a circular nose with a corner at $\chi=68^0$ and ω=0, while Fig. 24 shows the pressure distribution along smooth circular cones (solid line) and wedges (dotted line) for various apex angles [8,16]. From these figures it is apparent that, other things being equal (the flow regime, contour shape, etc.), the plane blunt body, in contrast to the axisymmetric (or a body with a sonic corner in contrast to a smooth one) introduces a greater disturbance into supersonic flow, and the resulting shock layer is thicker. Furthermore, in the case of blunt plates ω=0 and wedges $\omega \neq 0$ (plane flows), and also for bodies with a sonic corner (Fig. 25) a zone of overexpansion arises immediately after the blunt nose followed at the shoulder by a positive pressure gradient which increases rapidly with increasing χ. It follows that, all other things being equal, conditions more favorable to the generation of IFS are realized in the plane two-dimensional case or for bodies with a sonic corner.

Fig. 26 shows the main bow shock wave and IFS which arise in the supersonic zone in the case of flow about spherically blunted cones, which have a sonic corner ($\chi=30^0$; k=1.4) [17]. Results are shown for cones with semi vertex angles of $\omega=-5^0$, 0^0, 10^0 and incident Mach numbers of M_∞ = 4 (the solid curve) and M_∞ = 6 (dotted) curve. The intensity of the imbedded floating shock first rapidly increases and then gradually decreases with increasing distance from the blunt nose. In the cases cited above the angle through which the flow passing through the imbedded shock is deflected achieves a maximum of only a few degrees, while at a distance of some 30 to 40 nose radii this angle amounted to only a few seconds. V.F. Ivanov first computed tables of the locations of floating shocks [17]. It is interesting to note that when floating shocks formed, the shape and location of the main shock waves (in the region lying ahead of their intersection with secondary

shocks) coincided (for identical values of incident Mach number) for various half-angles of the cone in the range $-10^0 \leq \omega \leq +10^0$ (Fig. 27). This property is explained, apparently, by the substantial extent of the region of influence of a blunt nose, which, for such regimes of flow, includes a relatively large portion of the main shock wave. Fig. 28 illustrates the effect of the corner point on the position of the limiting characteristics.

An analogous situation regarding the region of influence is also observed for smooth blunt cones. Fig. 29 shows the coordinates of the shock wave for smooth cones with spherical noses. The coordinates of the point B, through which passes the characteristic bounding the region of influence of the nose are shown for various cone half-angles ω.

Fig. 30 shows examples of flow with IFS obtained by V.I. Kosarev for axisymmetric double-cone bodies with $\alpha = 0^0$ and 5^0 at $M_\infty = 6$ (k=1.4); these conditions insure isentropic compression of the flow at the juncture between the cones. Flow patterns (IFS are shown by dotted lines) and longitudinal surface pressure distributions are shown for the planes $\phi = 0, \pi/2, \pi$. Here, too, the generation of IFS is clearly seen when the conditions of a sufficiently thick shock layer and positive pressure gradient are present ($\alpha = 0^0$; $\alpha = 5^0$ at $\phi = 0, \pi/2$).

5. LOCAL SUPERSONIC ZONES

Recently, systematic calculations of "supercritical" and transonic rotational flows have been carried out by the Computing Center of the Academy of Sciences of the U.S.S.R. [37,38]. These apply to plane and axisymmetric bodies and are based on the method of "large particles" [31,32,37]. In this paper, without discussing the details of the method, we shall only be concerned with the formulation of the boundary conditions of the problem for this class of flows and present some computational results.

The development of the unsteady "large particles" method was stimulated by the works of F. Harlow [35] and others. We adhere to the "particle-in-cell" method. Nevertheless, it seems reasonable that, for gas dynamics problems, we should not confine ourselves to the discrete model of a continuous medium comprising a combination of particles of a cell of fixed mass. Instead, we consider continuous flows of "large particles" whose mass coincides with the mass of an Euler cell at a given instant of time. In this formulation each time cycle is divided into three stages ("Eulerian", "Lagrangian", and "Final"), with greater attention given to the development of a numerical algorithm which might be used for a wide class of problems concerned with motion of a compressible gas [31,32,35-38].

As a result, we have obtained some divergence form (conservative), dissipative-steady difference schemes which allow us to consider a wide class of transonic problems as well. Developments in this direction have been carried out since 1965.

5.1 "LARGE PARTICLES" METHOD

Let us briefly describe the main principles of the "large particles" method. The region of integration is covered by a fixed (over space) Euler

net composed of rectangular cells with sides Δx, Δy (or Δz, Δr in a cylindrical coordinate system).

In the first ("Eulerian") stage of calculations only those quantities change which are related to a cell as a whole, and the fluid is supposed to be momentarily decelerated. Hence, the convective terms of the form $\mathrm{div}(\phi\rho\vec{w})$, where $\phi = (1,u,v,E)$, corresponding to displacement effects, are omitted in the governing (initial) equations. Then it follows from the equation of continuity, in particular, that the density field will be "frozen" and the initial system of equations will be of the form

$$\rho \frac{\partial u}{\partial t} + \frac{\partial p}{\partial x} = 0, \quad \rho \frac{\partial v}{\partial t} + \frac{\partial p}{\partial y} = 0, \quad \rho \frac{\partial E}{\partial t} + \mathrm{div}(\rho\vec{w}) = 0 \qquad (5.1)$$

Here we have used both the simplest finite-difference approximations and, to improve the calculation stability, the schemes of the method of integral relations [36], in which "sweeping-through" approximations of the integrands with respect to rays (N = 3,4,5) are used [37].

In the second ("Lagrangian") stage we find mass flows ΔM^n across the cell boundaries at time $t^n + \Delta t$. At this stage we assume the total mass to be transferred only by a velocity component normal to the boundary. Thus, for instance,

$$\Delta M^n_{i+\frac{1}{2},j} = \left\langle \rho^n_{i+\frac{1}{2},j} \right\rangle \left\langle u^n_{i+\frac{1}{2},j} \right\rangle \Delta y \, \Delta t \quad , \quad \text{etc.} \qquad (5.2)$$

The brackets $\langle\ \rangle$ denote the values of ρ and u across the cell boundary. The choice of these values is extremely important since they substantially influence the stability and accuracy of the calculations. Consideration of the flow direction is essential to the various possible ways of writing down ΔM^n.

First and second order accurate representations of ΔM^n are considered. These are based on central differences, without account being taken of the flow direction, as well as by means of the discrete model of a continuous

medium comprising a combination of particles of a fixed mass in a cell.

Lastly, in the third ("Final") stage we estimate the final fields of the Euler flow parameters at the instant of time $t^{n+1} = t^n + \Delta t$ (all the errors in the solution are "removed"). As was pointed out, the equations at this stage are laws of conservation of mass M, momentum $\vec{P}$ and total energy E written down for a particular cell in the difference form

$$F^{n+1} = F^n + \Sigma \Delta F^n_{bdry} \qquad \text{where } F = (M, \vec{P}, E) \tag{5.3}$$

According to these equations, inside the flow field there are no sources or sinks of M, $\vec{P}$ and E and their variations in time Δt is caused only by interaction at the external boundary of the flow region.

It follows from the very character of the construction of the calculation scheme that a complete system of nonstationary gas dynamics equations is essentially solved here, while each calculation cycle represents a completed process in a given time interval. Consequently, the governing nonstationary equations, subject to the boundary conditions of the problem, are satisfied so that the real fluid flow at the time in question is determined.

Thus, the "large particles" method allows us to obtain the characteristics of nonstationary gas flows and as a consequence of their stability, the asymptotic steady state as well. Such an approach is especially applicable to problems in which a complete or partial development of physical phenomena with respect to time takes place. For example, in studying transonic gas flows and flows around finite bodies, flow in local supersonic zones and separation regions develop comparatively slowly while the major part of the field develops rather rapidly. Our investigation is wholly devoted to systematic calculations of a wide class of compressible flows involving transonic regime, discontinuities, separation and "injection".

The divergence forms of the differential and difference equations are

considered in the "large particles" method; the energy relation for total energy E is used; different kinds of approximations are used in the 1st and 2nd stages; additional density calculations are introduced in the final stage, which helps to remove fluctuations and makes it possible to obtain satisfactory results with a relatively small network (usually 1-2.5 thousand cells are used). All this results in completely conservative schemes, i.e., laws of conservation for the whole net region are an algebraic consequence of the difference equations. Fractional cells are introduced for the calculation of bodies with a curvature in the slope of the contour [37].

The investigation of these schemes (approximation problems, viscosity, stability, etc.) was carried out successively for the zero, the first and the second differential approximations [31,32,37]. These investigations show that the "large particles" method yields divergence-conservative and dissipative-steady schemes for "sweeping-through" calculations. This enables us to carry out stable calculations for a wide class of gas dynamics problems without introducing explicit terms with artificial viscosity. It may be of particular significance in studying flows around bodies with a curvature in the slope of the contour since the ways of introducing explicit terms with artificial viscosity are different for whole and fractional cells. Moreover, by varying only the second stage of the calculation procedure we can arrive at the conservative "particle-in-cell" method so that the calculational algorithm is of general use.

As for discontinuities the approximate viscosity in the scheme (dissipative terms in difference equations) results in stable calculations with a "smearing" of shock waves over several computational cells and the formation of a thick boundary layer near the body. It should be stressed that the magnitude of the approximate viscosity is proportional to a local flow

velocity and to the dimensions of the difference net, therefore its effect is practically evident only in zones with large gradients.

The boundary conditions of the problem were realized by introducing layers of "fictitious" cells along the region boundaries [31,32,37]. Conditions on the body closely approximate the "no-slip" condition. For example, in Fig. 31 where the density profile is given for the conditions of "no-slip" (dashed line) and vanishing of the normal component of velocity, identified "non-flow" (solid line), even in the vicinity of the body the difference between these two cases is insignificant and at some distance from the body it disappears entirely.

It turned out that the right hand "open" boundary of the region introduces the greatest distrubances in the calculation of transonic gas flows. To evaluate its influence and determine the optimum dimensions of the net, the calculations were carried out for nets of different sizes; "matching" of the flow fields was enforced by utilizing one of the internal columns as the initial one for a new field. Finally a comparison between the asymptotic (steady) state and experiment was made as well [31,32,37,38].

Fig. 32 shows the results of the calculations of a "super-critical" flow ($M_\infty = 0.9$) over regions of various extent, $\ell/R \simeq 2$ to 3 in the flow around a semi-finite cylinder (as if the body were "moved into" the stream). If the flow field ahead of the body is established rather quickly, then the flow downstream from the corner become steady only past $\ell/R \simeq 2$ to 3. The results of the calculations with a coarse net are shown in Fig. 32d while the region of Figs. 32a-32c (which utilize about 2.5 thousand nodes) is indicated by a dashed line.

A comparison is given in Fig. 33 between the results of the calculations (solid lines) and analytical data for the asymptotic steady state (dashed

line) for a sonic flow around the same body [31,32]. In this figure "1" is the sonic line, "2" the limiting characteristic curve, "3" is the line showing the departure of the velocity vector from the horizontal, and "4" is the shock wave. It should be noted that good agreement is observed with the analytic data already at a distance of 2-3 radii from the body.

5.2 CALCULATION OF TRANSONIC AND "SUPERCRITICAL" FLOWS

Some computational results obtained by the "large particles" method [37,38] for transonic flows around two-dimensional and axisymmetric bodies will now be described. For purposes of this discussion the supercritical regimes of transonic flows around bodies will be characterized by the value of the critical Mach number of the oncoming flow M_∞^* (i.e., when a sonic point first develops on the body) as well as by the extent of the local supersonic zone (as compared to a characteristic dimension of the body) and by its intensity (say the maximum supersonic velocity $\overline{M}$ realized in the zone).

Fig. 34 (series 1 - 8) presents the flow field patterns (lines M = constant) for a 24% circular arc profile ($\nu = 0$) extending from purely subsonic ($M_\infty = 0.6$) to supersonic regimes ($M_\infty = 1.5$). Successive flow fields for increasing M_∞ depict transition through the critical Mach number (here $M_\infty^* = 0.65$) and the formation and development of a local supersonic zone. The supercritical flow around this profile is observed for $0.7 < M_\infty < 1$ (Figs. 34 :2-7). One can distinctly see the position of the shock in the region of crowded M = constant lines which, together with the sonic line, bound the local supersonic flow. The region of subsonic velocities is located behind the shock wave. When the velocity of the oncoming flow increases, the flow disturbances produced by the body die out at a large distance from

the body. With $M_\infty \geq 0.9$ the zone becomes considerable both in size and in intensity (supersonic velocities up to M = 1.7 to 1.8 are attained) and in case of a sonic flow (Fig. 34.7) lines of the level M = 1 extend to infinity.

The asymmetry of the whole flow pattern is noticeable (even at purely subsonic velocities - Fig. 34.1) which results from non-potentiality of the flow (supercritical regimes) and from the presence of viscous effects as well (formation of a wake behind the body).

In the case of supersonic flow past this profile (Fig. 34.8, $M_\infty = 1.5$) a shock wave developes ahead of the body which bounds the disturbed region. Behind the wave, subsonic velocities occur in the vicinity of the axis of symmetry away from which the flow velocity along the contour of the body increases and, as a result, a "terminal" shock occurs near the stern of the body.

For comparison the results of calculations by the above method for flow around a 24% axisymmetric "spindlelike" body ($\nu = 1$) are given in Fig. 35 with $0.8 < M_\infty < 2.5$. In this case a critical regime already occurs at $M_\infty^* = 0.86$; local supersonic zones as compared to the plane case are less developed and of weaker intensity (for example, values of $M \simeq 1.3$-1.4 are realized), although, naturally, the main features of a transonic flow are quite evident (see also [38]).

In Fig. 36 a comparison is given between the flow fields calculated by the above method (solid line) and those of the Wood and Gooderum experiment (dashed line) for subcritical (Fig. 36a, M = 0.725) and supercritical (Fig. 36b, $M_\infty^* = 0.761$) flows around a 12% profile (results of both the calculations and the experiment indicate $M_\infty^* = 0.74$).

As compared to the corresponding plane cases with the same value of δ it can be seen that, in axisymmetric flows, an increase is seen in the critical

Mach number (with $\delta = 12\%$, from 0.74 to 0.89, and from 0.65 to 0.86 for $\delta = 24\%$). In axisymmetric flow local supersonic zones are of smaller size and lower intensity, for instance, the maximum Mach number in these zones is $M \simeq 1.2$ for $\nu = 1$ as compared to $\overline{M} = 1.5$ for $\nu = 0$ when $\delta = 12\%$, and $\overline{M} = 1.3$: 1.7 when $\delta = 24\%$. However greater asymmetry of the flow picture about the vertical axis is observed for axisymmetric bodies; behind the body we find a stronger wake, which exerts quite a marked influence on the flow picture, and finally, the shock layer is considerably narrower in supersonic axisymmetric flow.

Analysis of internal check tests as well as the results of various comparisons indicate that the computational error of the "large particles" method usually does not exceed several per cent. These calculations were carried out using a Soviet, BESM-6 computer; the time of the calculation in this case did not exceed an hour.

Some numerical results obtained by the large particle method for flow past more complicated types of bodies will now be considered. In Fig. 32 we have plotted the M = constant lines for supercritical flow past a semi-infinite cylindrical block (here, $M_\infty^* \simeq 0.70$, which is in good agreement with the experimental value $M_\infty^* = 0.69$ obtained by Stanbrook [40]) while Fig. 37 refers to the case of sonic flow past a space vehicle of the Apollo type. The streamlines, bow shock wave and sonic line in supersonic flow past a short cylindrical body and a sphere are shown in Fig. 38. These numerical results clearly indicate the formation, behind "badly streamlined" bodies (Figs. 37 and 38), of closed recirculation zones, localized behind the tail, which are isolated from the external flow by a contact surface (marked by a dashed line in Fig. 38). The flow in the recirculation zones is strongly subsonic and extremely rarefied (i.e., both the gas density and pressure are small in them).

An important pratical application of the large partical method is described by near sonic flow ($M_\infty \simeq 1$) past a body that has a jet (with parameters M_c, p_c, u_c, v_c) "blown out" opposite to the main flow, thus changing the entire flow field. In this case, auxiliary conditions for the jet flow must be prescribed, usually sonic velocity, with the jet parameters specified in appropriate cells on the body surface. The field of constant Mach number contours are shown in Fig. 39a, for sonic flow ($M_\infty = 1.0$) past a sphere which has an axial sonic jet ($M_c = 1.0$; $\rho_c = 2.9$, $u_c = 1.0$, $v_c = 0$), issuing upstream from a nozzle located on its axis of symmetry; Fig. 39b gives corresponding results for supercritical flow at $M_\infty = 0.9$. In the presence of a jet the flow around the body becomes much more complicated and is unsteady in the mixing region. The flow field splits into two sub-regions; the gas coming from the jet passes through one of them, and the external flow through the other. The trend towards this division may be seen in Fig. 39a, and becomes even more evident in the supercritical case (Fig. 39b). This demarcation is given by the contact surface (shown by the dashed line in Fig. 39b) which separates the external flow from the injected gas. A separated wake is also formed behind the body.

6. ON THE QUESTION OF EXTREMALITY OF THE ENTROPY ON THE STAGNATION STREAMLINE IN THREE-DIMENSIONAL FLOW

Of great interest in three-dimensional supersonic flow is the question as to whether the stagnation streamline (streamline arriving at the body) passes through a point on the shock where it is orthogonal to the velocity vector.

It has been shown in [18] that if the entropy does not have a maximum on the surface of an axisymmetric body in supersonic three-dimensional flow, then the vorticity on the body surface is a discontinuous function of the angle of attack. This property was found under the assumption that the curvature of the shock was finite at its point of intersection with the axis of symmetry (it was later established that this assumption is always true).

An investigation of the local three-dimensional flow in the neighborhood of the stagnation point on a body showed that the vorticity is generally not bounded on the body surface [19]. In the general case of flow around a body with a detached shock, an analogous result has been obtained under the assumption of the existence of a stagnation streamline in [20].

THEOREM 24. For the normal derivative of the velocity on a body surface to be bounded, it is necessary that conditions for the existence of an extremum in the entropy be satisfied on the stagnation streamline.

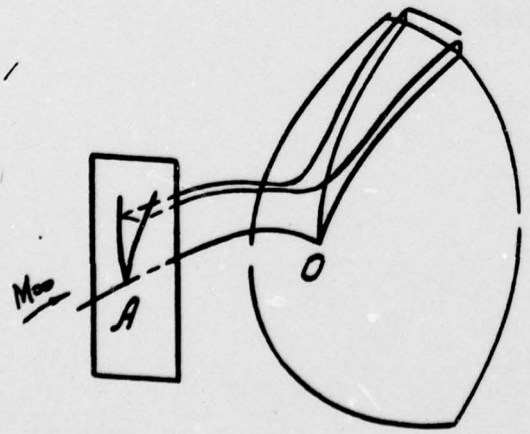

Figure 40. Special coordinate system generated by the stagnation streamline.

If these conditions are not satisfied, then the body surface is almost everywhere the envelope of surfaces of equal velocity magnitude; a weak discontinuity is propagated along two body streamlines which emerge from the stagnation point (Fig. 40). The construction of an appropriate example in [20] showed that the extremality of the entropy on the stagnation streamline is generally insufficient for the boundedness of the normal velocity derivative on the body surface.

It should also be noted that an approximate solution of the problem of three-dimensional hypersonic flow around a body [21] has shown that the entropy does not take on a maximum value on the body surface. An analogous deduction has been made in [22] from an experimental investigation of the problem. Numerous calculations ([17] et al.) of the flow around axisymmetric bodies at angles of attack over a wide range of flow conditions ($1 < M_\infty < 20$, $0 < \alpha < 25^0$) have shown that the difference in entropy on the body surface from the maximum value is of the same order as the computational error.

Therefore, although the connection between the extremum of the entropy on the stagnation streamline and the flow properties at the body surface has indeed been established in the papers cited, the question posed herein remains open for a rigorous theoretical analysis.

REFERENCES

1. G. Bruhn and W. Haack, "Ein Charakteristikenverfahren fur dreidimensionale instationare Gasstromungen," ZAMP Vol. 9b, Nos. 5-6, 1958, pp. 173-190.

2. L.I. Sedov, *Two-Dimension Problems of Hydro- and Aerodynamics*, Interscience, New York, 1965.

3. R. Von Mises, *Mathematical Theory of Compressible Fluid Flow*, Academic Press, 1958.

4. E.G. Shifrin, "On the Direct Problem of Flow Around a Profile With a Detached Shock," Dokl. AN SSSR, Vol. 171(3), 1967, pp. 550-553.

5. R.G. Barantsev, *Lectures on Transonic Gasdynamics*, Leningrad Univ. Press, 1965.

6. A.A. Nikol'skii and G.I. Taganov, "Gas Motion in a Local Supersonic Zone and Some Conditions Spoiling Potential Flow," PMM* Vol. 10, No. 4, 1946, pp. 481-503.

7. E.G. Shifrin, "Some Properties of Symmetric Flow Around a Profile with a Detached Shock," Izd. AN SSSR, Mekh. Zhidk. i Gaza, No. 5, 1966, pp. 99-101.

8. O.M. Belotserkovskii, "Flow Around a Symmetric Profile with a Detached Shock," Sov. J. Appl. Math & Mech.**, Vol. 22, No. 2, 1958, pp. 279-296.

9. O.M. Belotserkovskii and E.G. Shifrin, "On the Inclination of the Sonic Line to the Shock in Axisymmetric Flow," Izd. AN SSSR, Mekh. Zhidk. i Gaza, No. 5, 1967, pp. 110-112.

10. W. Sears, ed., *General Theory of High Speed Aerodynamics*, Princeton Univ. Press, N.J., 1954.

11. E.G. Shifrin, "Plane Vortex Flow in the Neighborhood of a Point of Orthogonality of the Sonic Line to the Velocity Vector," Izv. AN SSSR, Mekh. Zhidk. i Gaza, No. 6, 1966, pp. 144-146.

12. S.V. Fal'kovich, "On the Theory of the Laval Nozzle," PMM Vol. 10, No. 4, 1946, pp. 503-513.

---

* PMM - Prikl. Mat. i Mekhan.

** Translation of PMM by Pergamon Press.

13. V.I. Fidrus and E.G. Shifrin, "Axisymmetric Vortical Flow in the Neighborhood of a Point of Orthogonality of a Sonic Surface to the Velocity Vector," Izv. AN SSSR, Mekh. Zhidk. i Gaza, No. 1, 1967, pp. 91-93.

14. V.I. Fidrus and E.G. Shifrin,"Three-Dimensional Vortical Flow in the Neighborhood of a Point of Orthogonality of a Sonic Surface to the Velocity Vector, Izv. AN SSSR, Mekh. Zhidk. i Gaza, No. 3, 1968, pp. 121-123.

15. E.G. Shifrin, "On a Condition to Spoil the Domain of Continuous Supersonic Flow in the Flow Around a Profile with a Detached Shock," Dokl. AN SSSR, Vol. 176, No. 4, 1967, pp. 797-800.

16. P.I. Chushkin, "Blunt Body of Simple Shape in a Supersonic Gas Flow," Sov. J. Appl. Math. & Mech., Vol. 24, No. 5, 1960, pp. 1397-1403.

17. O.M. Belotserkovskii, ed., *Supersonic Gas Flow Around Bodies, Theory and Experiment**, Trudy Vychisl. Tsentr. Moscow, 1967.

18. M.D. Ladyzhenskii, *Three-Dimensional Hypersonic Gas Flow*, Mashinostroenie, 1968.

19. W.D. Hayes, "Rotational Stagnation Point Flow," J. Fluid Mech., Vol. 19, No. 3, 1964, pp. 366-374.

20. E.G. Shifrin, "On Extremality of the Entropy at the Stagnation Streamline in Three-Dimensional Flow," Sov. J. Appl. Math. & Mech., Vol. 31, No. 3, 1967, pp. 618-620.

21. W.D. Hayes, "Hypersonic Stagnation Region Flows with Asymmetry," Archiv. Mech. Stosowanej, Vol. 18, No. 6, 1966, pp. 797-804.

22. A.I. Glagolev and A.I. Zubkov, "Experimental Investigation of the Extremality of the Entropy on the Stagnation Streamline in Three-Dimensional Flow Around Bodies," Izv. AN SSSR, Mekh. Zhidk. i Gaza, No. 1, 1968, pp. 90-95

23. A.A. Dorodnitsyn, "On a Method of Numerical Solution of Non-linear Aerodynamics Problems," Trudy III All-Union Math. Congr., Moscow, 1965, No. 3, AN SSSR Press, 1958, pp. 447-453.

---

* This book is translated by NASA TT,F-453, 1967. (See also: "Numerical Methods for Solving Problems of Mechanics of Continuous Media," Ed. O.M. Belotserkovskii, Comp. Center Ac. Sciences USSR, Moscos, 1969 NASA TT, F-667, 1972.)

24. O.M. Belotserkovskii, A. Bulekbaev and G. Grudnitskii, "Algorithms of Numerical Schemes of the Integral Relations Method for the Analysis of Mixed Gas Flows," USSR J. Comp. Math. & Math. Phys. * , Vol. 6, No. 6, 1966, pp. 162-184.

25. R. Vaglio-Laurin, "Transonic Rotational Flow Over a Convex Corner," J. Fl. Mech., Vol. 9, No. 1, 1960, pp. 81-103.

26. O.M. Belotserkovskii, E.S. Sedova and F.V. Shugaev, "Supersonic Flow Over Bodies of Revolution With a Break in the Generator," USSR J. Comp. Math. & Math. Phys., Vol. 6, No. 5, 1966, pp. 210-217.

27. S.V. Fal'kovich and I.A. Chernov, "Sonic Gas Flow Around Bodies of Revolution," Sov. J. Appl. Math. & Mech., Vol. 28, No. 2, 1964, pp. 342-347.

28. F.D. Popov, "On a Single Scheme of the Integral Relations Method in the Problem of Supersonic Flow Around Blunt Bodies," Zh. Techn. Fiz., Vol. 36, No. 2, 1966, pp. 239-245.

29. P.I. Chushkin, "Computation of Some Sonic Gas Flows", PMM Vol. 21, No. 3, 1957, pp. 353-360.

30. Yu. A. Dunaev, ed., *Aerophysical Supersonic Flow Investigations*, Nauka Press, 1967.

31. O.M. Belotserkovskii, Yu. M. Davidov, "The Use of Unsteady Methods of 'Large Particles' for Problems of External Aerodynamics," Preprint Vych. Tsentr. AN SSSR, 1970.

32. O.M. Belotserkovskii, Yu. M. Davidov, "A Non-Stationary 'Coarse Particle' Method for Gas Dynamic Computations," USSR J. Comp. Math. & Math. Phys., Vol. 11, No. 1, 1971, pp. 241-271.

33. E.G. Shifrin, "Formation of Floating Shock Waves for Flow Past Profiles with Broken Contours," Sov. J. Appl. Math. & Mech., Vol. 34, No. 6, pp. 1097-1107.

34. O.N. Katskova, I.N. Naumova, Yu. D. Shmiglevskii, N.P. Shulishnina, "Experiments to Calculate Plane and Axisymmetric Supersonic Flow of a Gas by the Method of Characteristics," Trudy Vychisl. Tsentr., Moscow, 1961.

35. F.H. Harlow, "The Particle-in-Cell Computing Method for Fluid Dynamics," *Methods in Computational Physics*, Vol. 3 (B. Alder, S. Fernbach, M. Rotenberg, eds.) Academic Press, New York, 1964.

---

* Pergamon Press translation of Zh. Vychisl. Matem. i Matem. Fiz.

36. O.M. Belotserkovskii, P.I. Chushkin, "A Numerical Method of Integral Relation," USSR J. Comp. Math. & Math. Phys., Vol. 2, No. 5, 1962, pp. 823-858.

37. O.M. Belotserkovskii, ed., *Numerical Investigation of Modern Problems in Gas Dynamics*, Nauka Press, Moscow, 1974.

38. O.M. Belotserkovskii, Yu. M. Davidov, "Computation of Transonic 'Supercritical' Flows by the 'Coarse Particle' Method," USSR J. Comp. Math. & Math. Phys., Vol. 13, No. 1, 1973, pp. 187-216.

39. G.P. Wood and P.B. Gooderum, "Investigation With an Interferometer of the Flow Around a Circular-Arc Airfoil at Mach Numbers Between 0.6 and 0.9," Natl. Advisory Comm. Aeron. (NACA) Tech. Note No. 2801, U.S. Govt. Printing Office, Washington, D.C., October 1952.

40. A. Stanbrook, "Experimental Pressure Distribution on a Plane-nosed Cylinder at Subsonic and Transonic Speeds," ARC RM-3425, London, 1966.

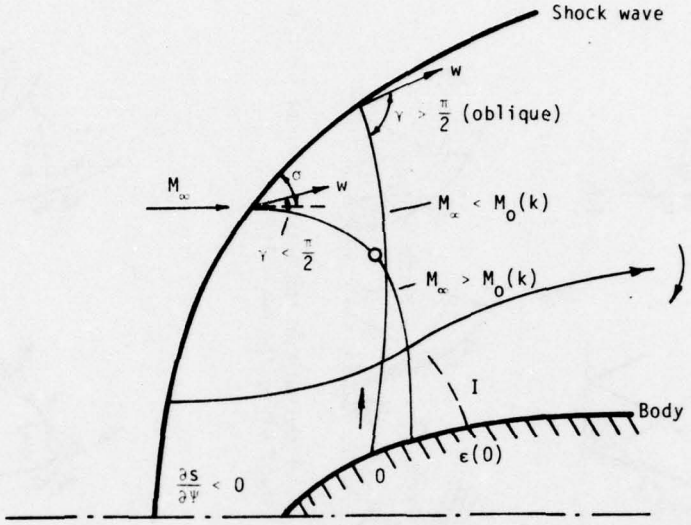

Fig. 1. General features of the flow around a body with a detached bow shock.

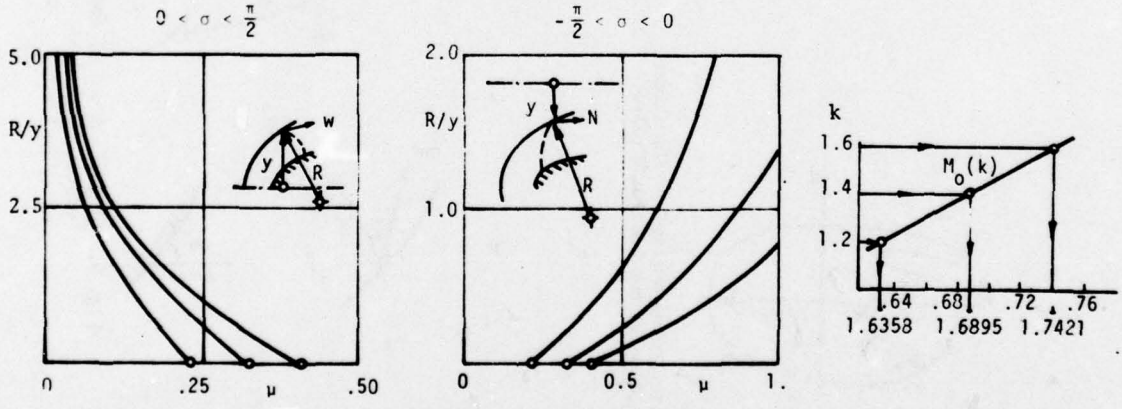

Fig. 2. Ratio of the shock curvature to its distance from the axis of symmetry at the sonic point as a function of the relative speed coefficient, $\mu = \frac{\lambda_\infty - 1}{\sqrt{(k+1)/(k-1)} - 1}$

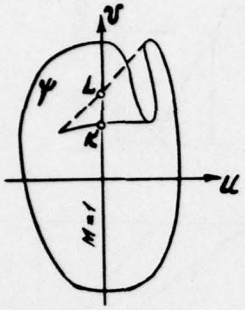

Fig. 3. Multisheeted surface of the stream function in the hodograph plane.

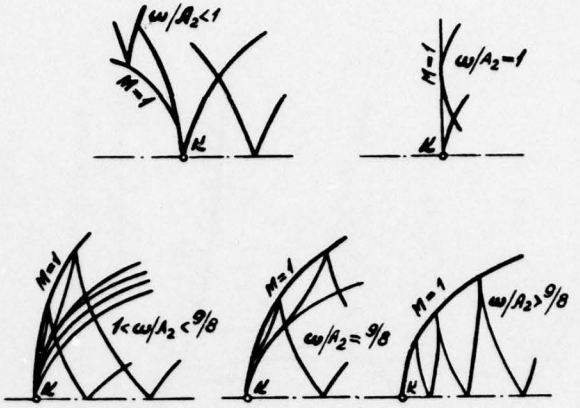

Fig. 4. Nature of the flow in the neighborhood of point K as a function of the parameter ω/A_2.

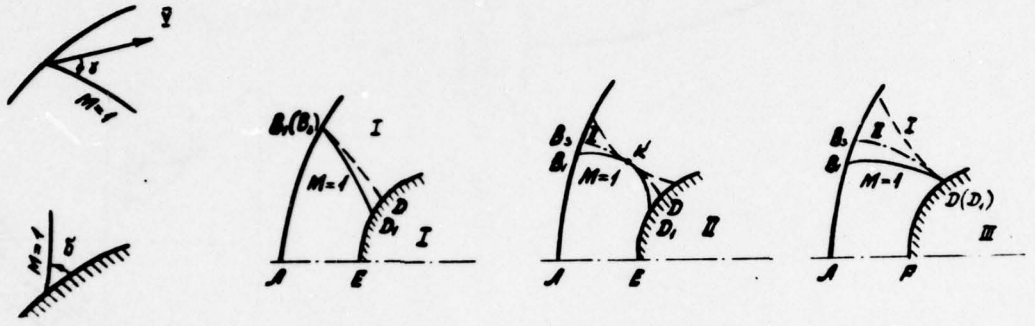

Fig. 5. Classification of domains of influence of bluntness for two-dimensional and axisymmetric bodies. Type I with $\gamma \leq \pi/2$, $\delta < \pi/2$; type II with $\gamma < \pi/2$, $\delta < \pi/2$; type III with $\gamma < \pi/2$, $\delta \geq \pi/2$

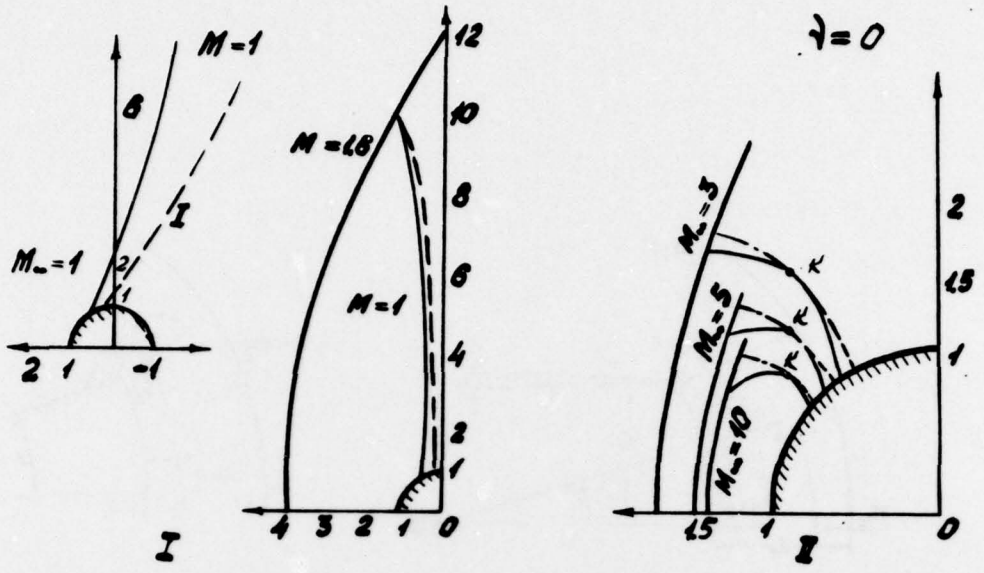

Fig. 6. Domains of influence in flows of a perfect gas (k = 1.4) around a circular cylinder: I for $M_\infty < 1.69$; II for $M_\infty > 1.69$.

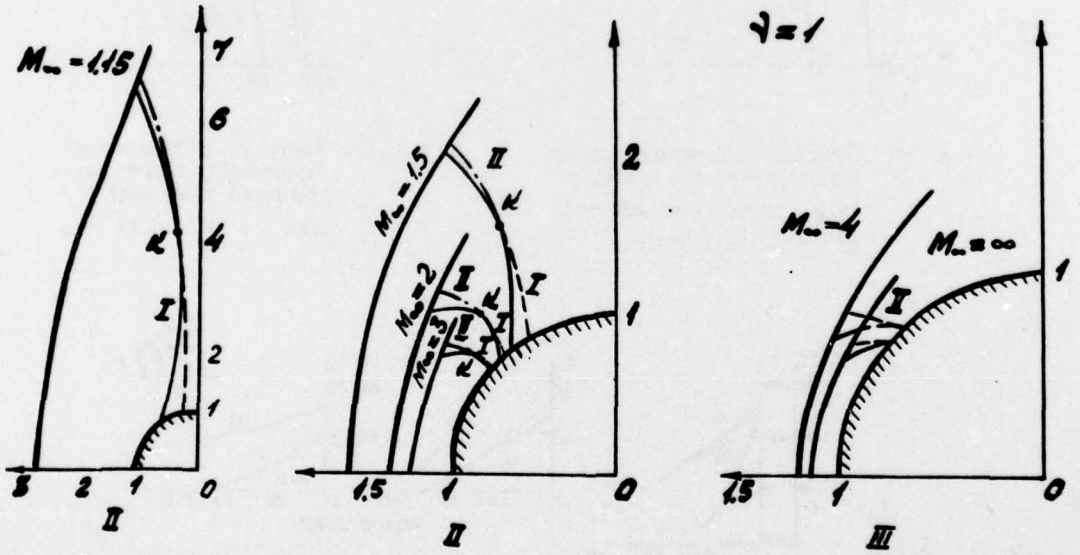

Fig. 7. Domains of influence in flows of a perfect gas (k = 1.4) around a sphere: II for $1.1 < M_\infty < M_2 = 3.7$; III for $3.15 < M_\infty < \infty$.

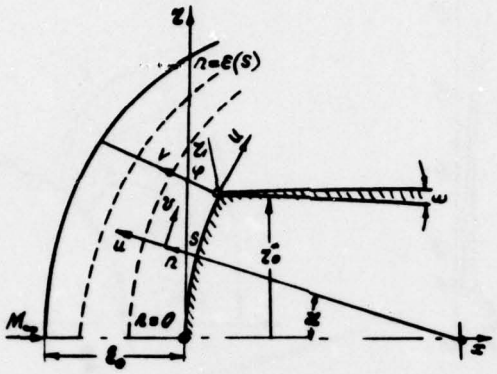

Fig. 8. Computational mesh for Scheme 1 of the Method of Integral Relations.

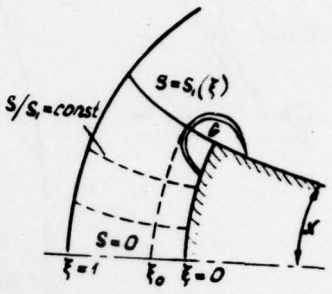

Fig. 9. Computational mesh for Scheme II of the Method of Integral Relations.

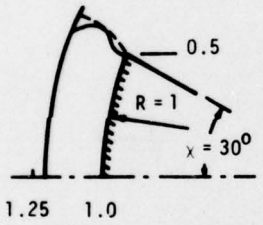

Fig. 10. Geometry of supersonic flow with $M_\infty = 4$ past a spherically-capped reversed cone of $\chi = 30^\circ$ half angle.

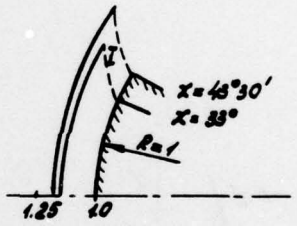

Fig. 11. Geometry of flow around spherically-capped noses of reversed cones with $M_\infty = 10$ and $\chi = 33^\circ$ and $43^\circ30'$.

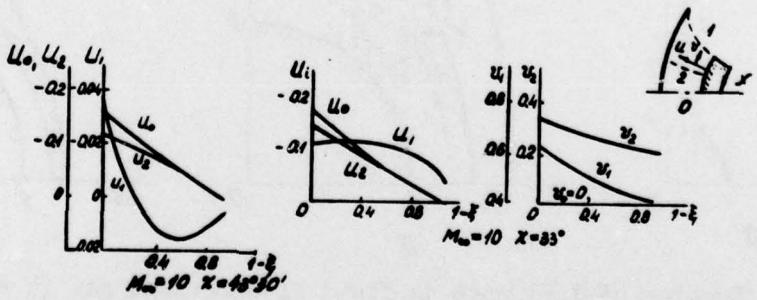

Fig. 12. Distribution of the normal, u_i, and tangential, v_i, velocity components across the shock layer of the bodies of Fig. 11. calculated from Scheme II, along the axis of symmetry i=0, along the limiting characteristic, i = 1 and the intermediate line, i = 2.

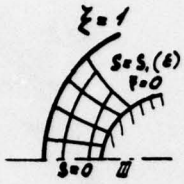

Fig. 13. Computational mesh for Scheme III of the Method Integral Relations.

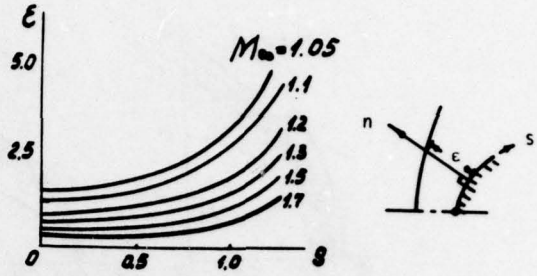

Fig. 14. Geometry of Detached Bow Shock in supersonic flow of a perfect gas (k = 1.4) past a sphere.

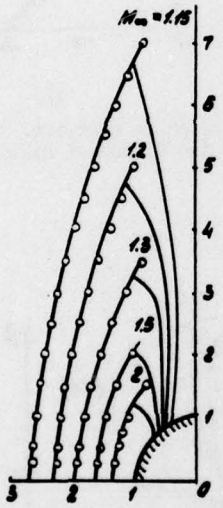

Fig. 15. Comparison of numerical results with experiment (points) of Bedin and Mishin [30] for supersonic flow (k = 1.4) past a sphere.

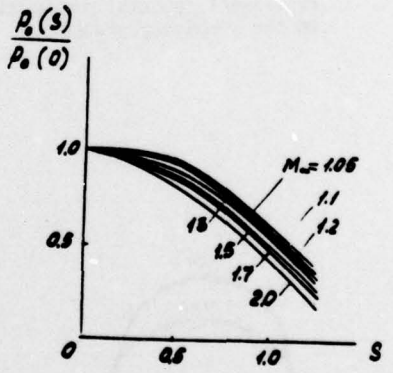

Fig. 16. Calculated surface pressure distribution along a sphere with k = 1.4.

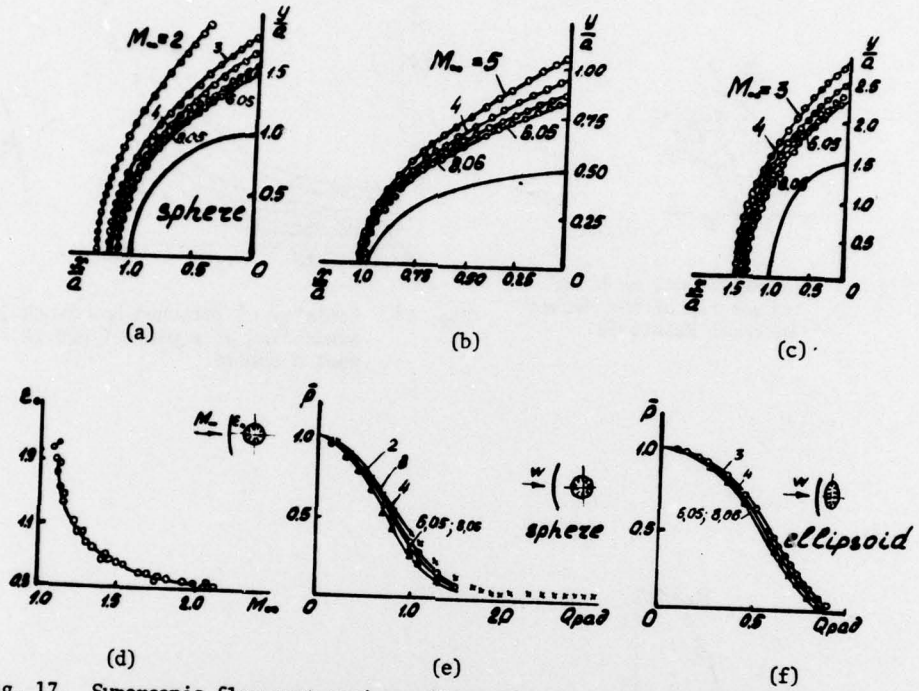

Fig. 17. Supersonic flow *past various ellipsoids:* Comparison of numerical results with experiment (points) of Maslennikov, et al [30] in (d) and of Riabinkov [17] in the remaining graphs.

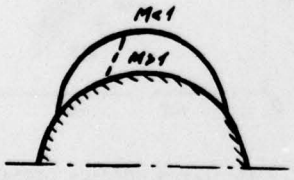

Fig. 18. Local supersonic "Zone I" in a subsonic potential flow according to Nikol'skii and Taganov [5].

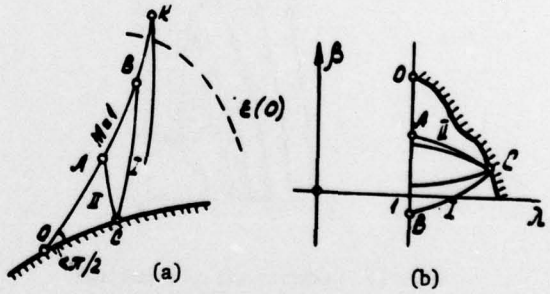

Fig. 19. (a) Zone III in the physical plane.
(b) Mapping of Zone III in the hodograph plane.

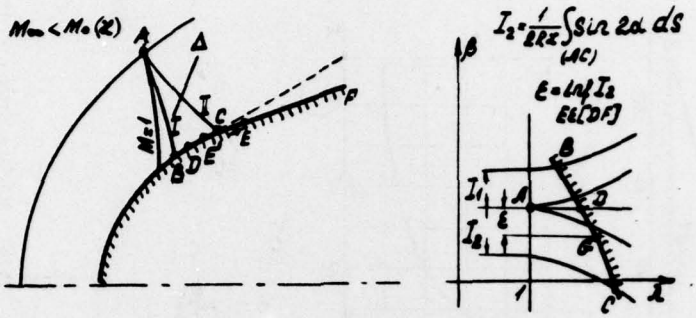

Fig. 20. The collapse of the continuous supersonic flow in the characteristic triangle Δ which adjoins the minimal domain of influence as the angle of the infinite blunted wedge increases.

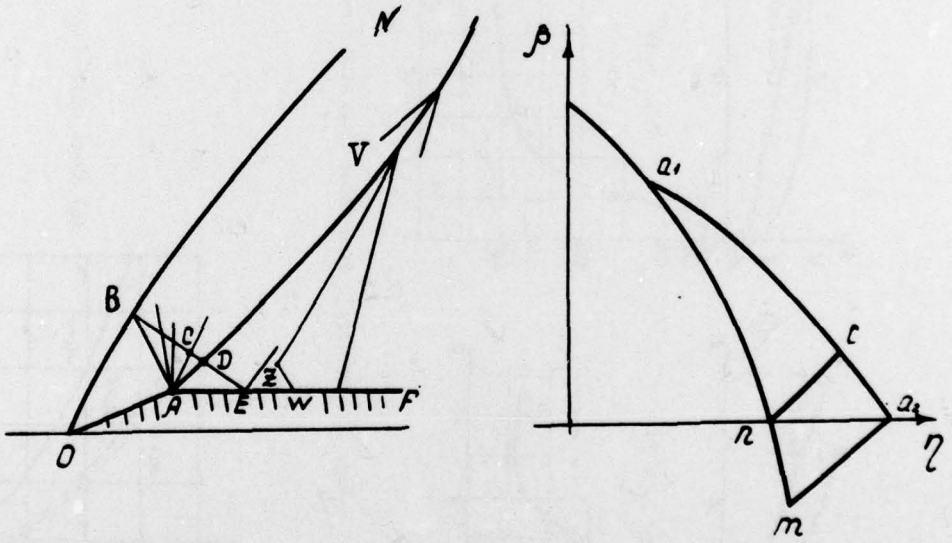

Fig. 21. Supersonic flow past a wedge-slab body with attached shock wave: AB, AC, AD - characteristics of the first family, BE of the second family.

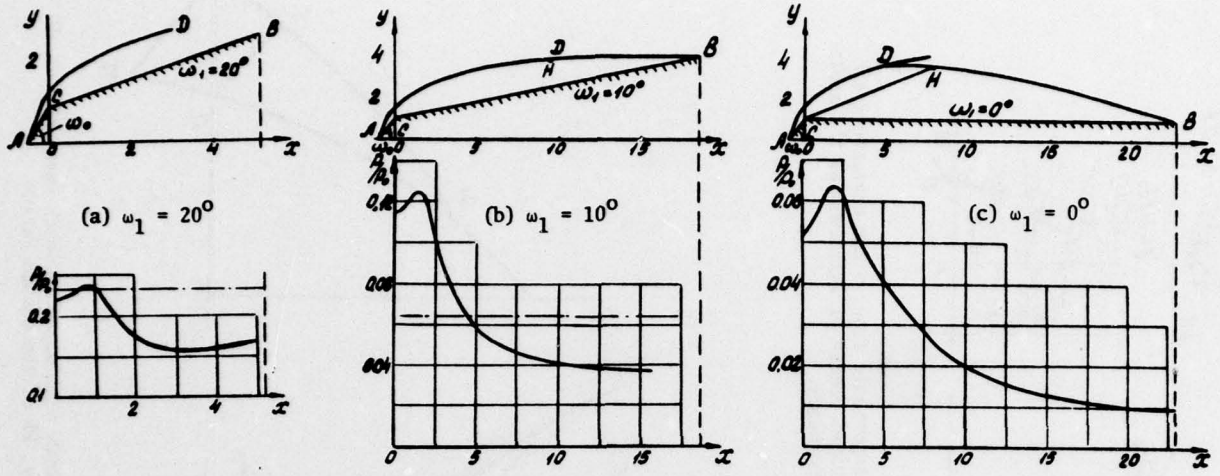

Fig. 22 Supersonic flow about truncated cones, $M_\infty = 100$, $k = 1.4$ and $\omega_o = 54.5^o$.

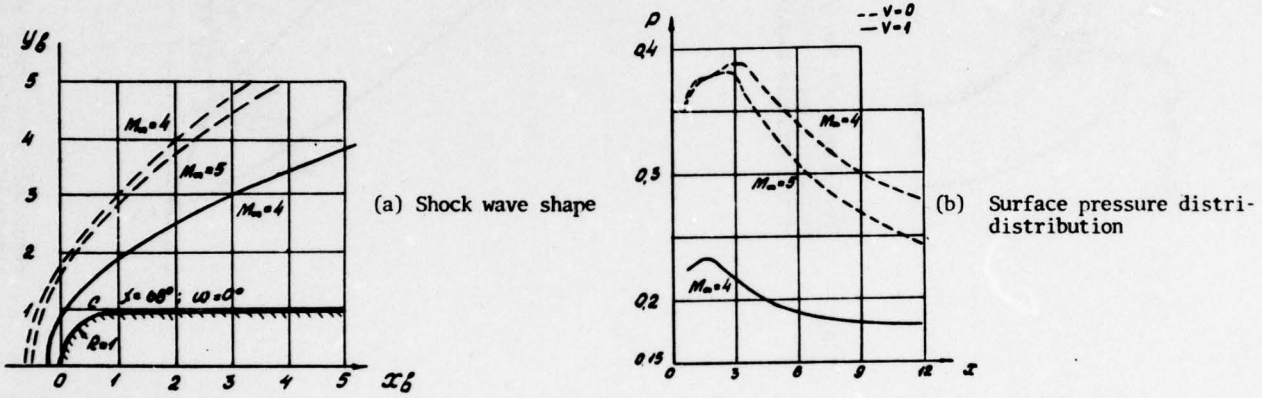

Fig. 23 Two-dimensional ($\nu = 0$) and axisymmetric ($\nu = 1$) supersonic flow past a straight line profile with a circular nose and corner at $\chi = 68^o$.

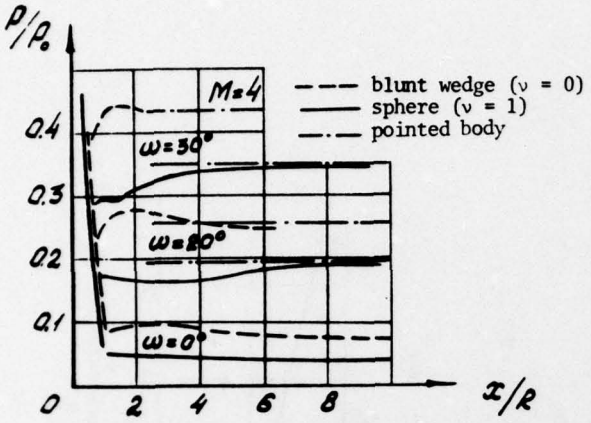

Fig. 24. Surface pressure distribution along cones and wedges with various nose blunting.

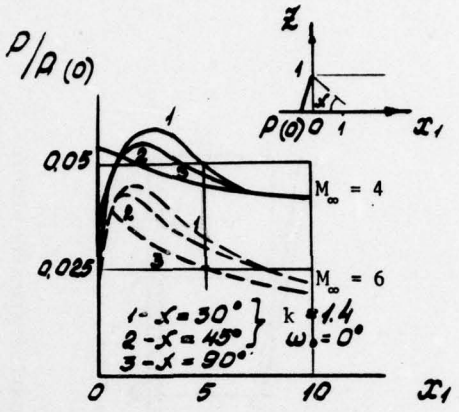

Fig. 25. Surface pressure distribution over spherically blunted cylinders of various segment semi-angles χ having a sonic corner.

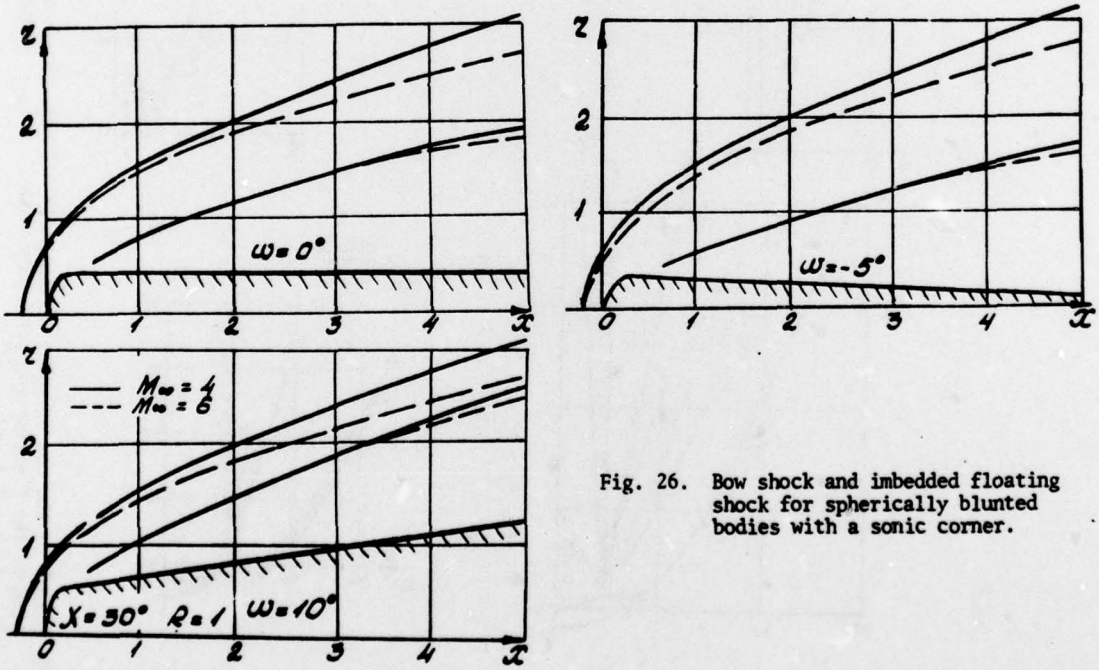

Fig. 26. Bow shock and imbedded floating shock for spherically blunted bodies with a sonic corner.

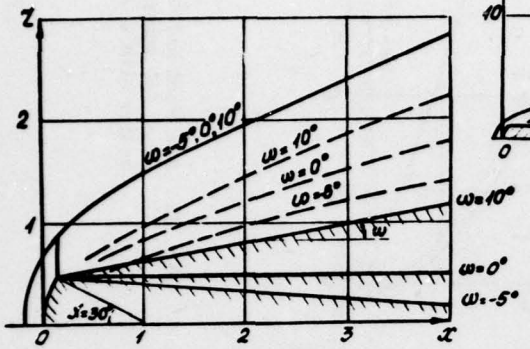

(a) $M_\infty = 4$, $\chi = 30^\circ$

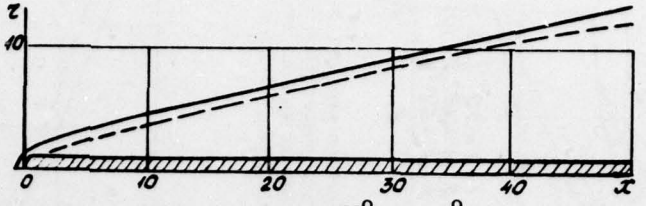

(b) $M_\infty = 5.8$, $\chi = 33^\circ$, $\omega = 0^\circ$

Fig. 27 Supersonic flow around spherically blunted cones with k = 1.4.

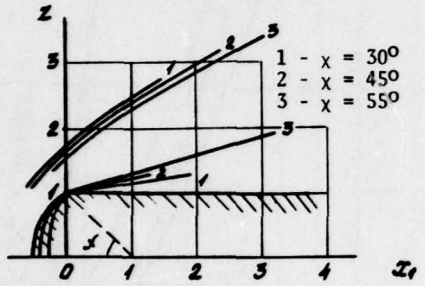

Fig. 28 Effect of the corner point on the position of the limiting characteristic with $M_\infty = 4$; k = 1.4 and $\omega = 0^\circ$.

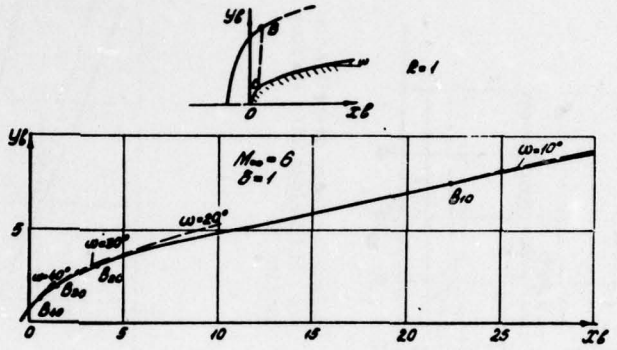

Fig. 29 Coordinates of the shock waves on spherically blunted cones at $M_\infty = 6$.

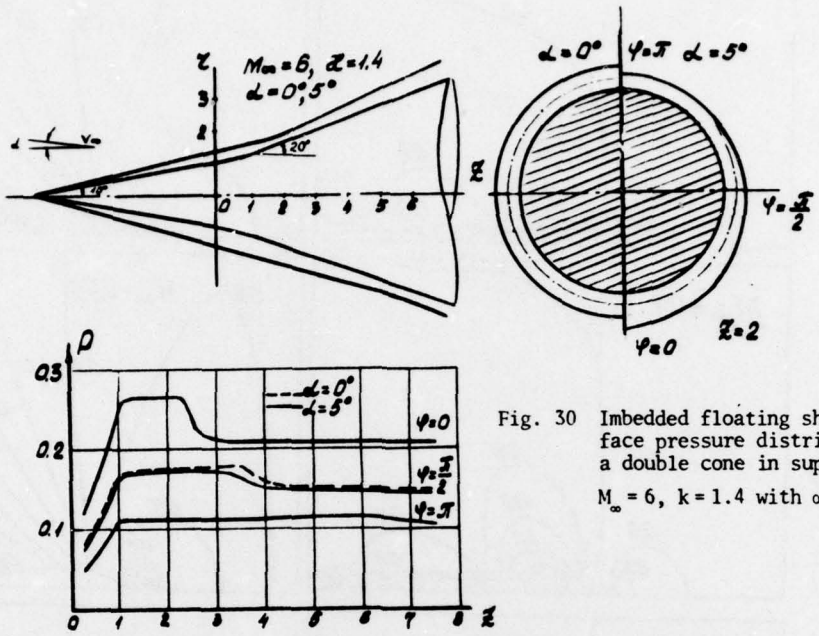

Fig. 30 Imbedded floating shock and surface pressure distribution over a double cone in supersonic flow, $M_\infty = 6$, $k = 1.4$ with $\alpha = 0^o$ and 5^o.

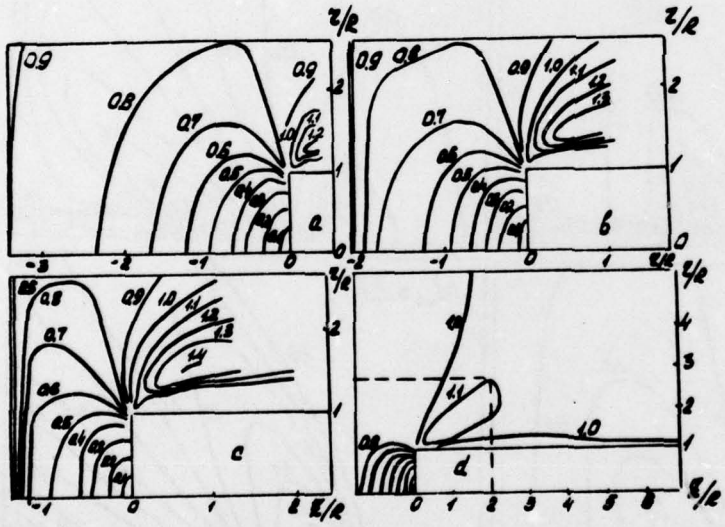

Fig. 32 Lines of constant Mach number (isotachs) in supercritical flow ($M_\infty = 0.9$) around flat-faced cylinders of various lengths: (a) $\ell/R = 0.56$, (b) $\ell/R = 2.0$, (c) $\ell/R = 2.72$, (d) $\ell/R = 7$.

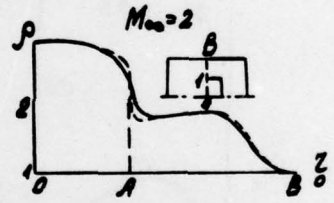

Fig. 31 Density profiles for boundary conditions of no-slip (---) and vanishing of velocity component normal to surface (——).

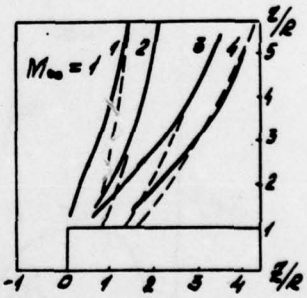

Fig. 33 Comparison of numerical results (—) with the asymptotic steady state [31,32] for sonic flow past a flat-faced cylinder: 1 - sonic line, 2 - limiting characteristics, 3 - locus of horizontal velocity vector, 4 - shock wave.

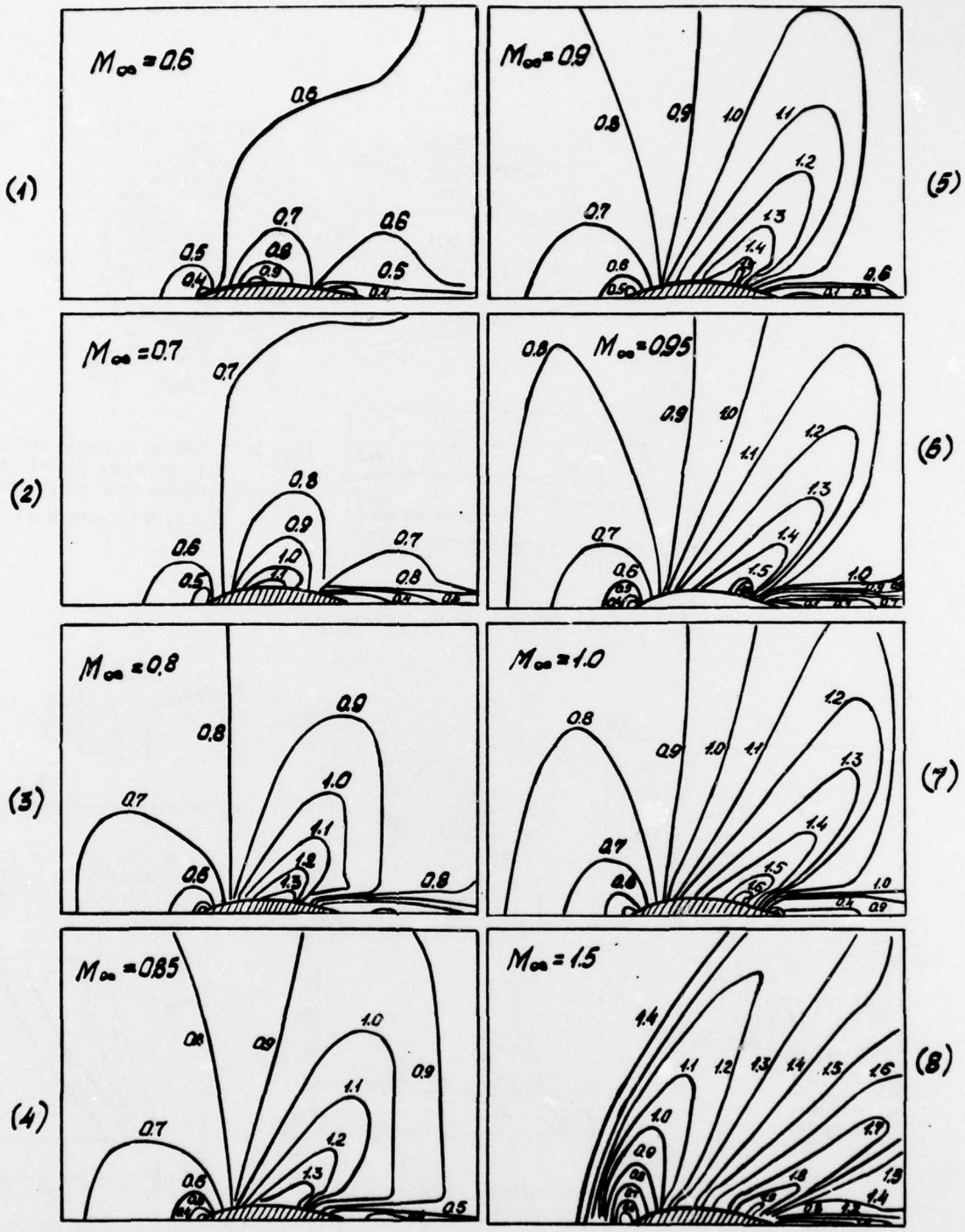

Fig. 34 Isotachs in transonic flow around a two-dimensional 24 per cent circular arc profile; critical Mach number, $M_\infty^* = 0.65$.

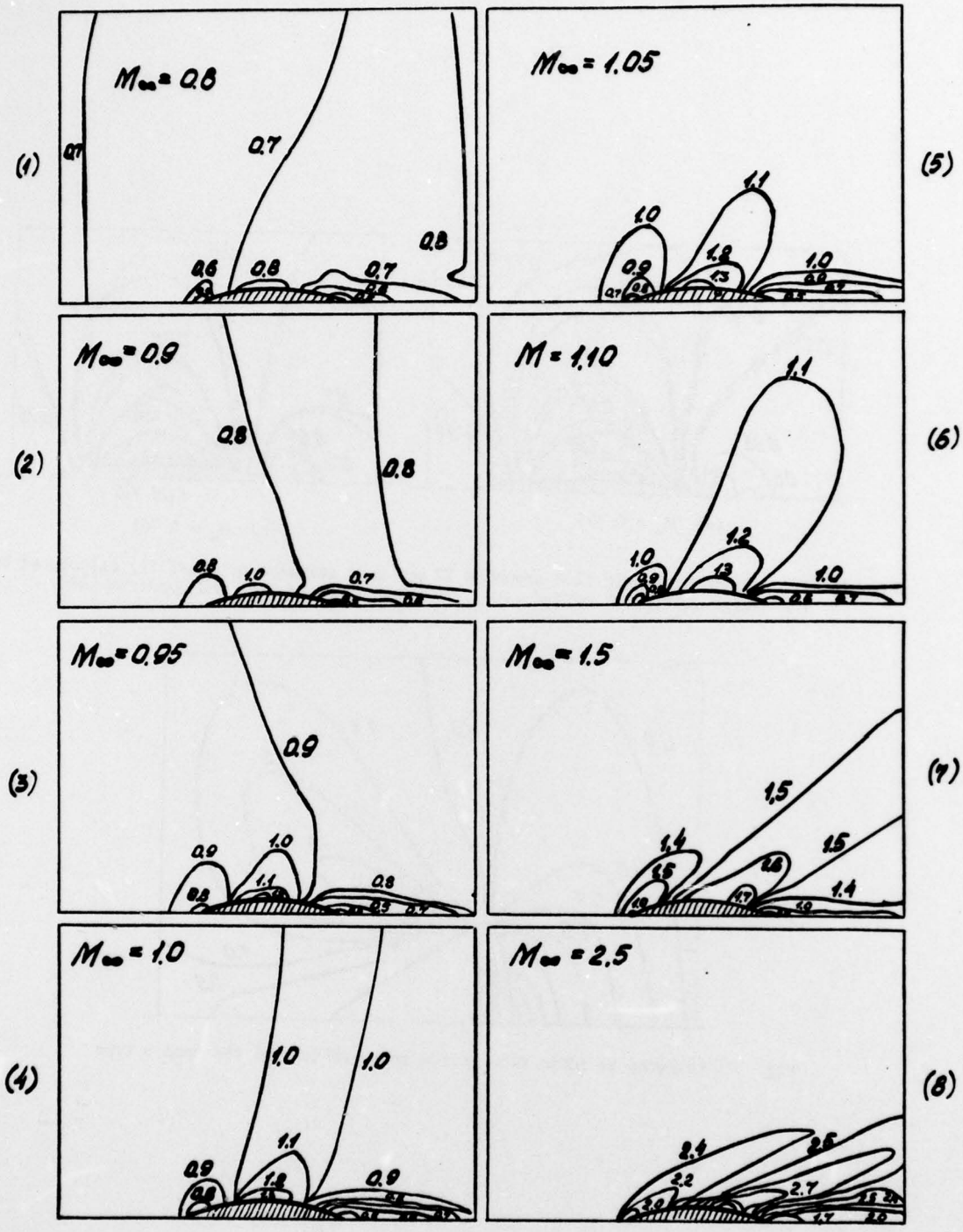

Fig. 35 Isotachs in transonic flow around a 24 per cent axisymmetric body (generated by revolution of a circular arc profile); critical Mach number, $M_\infty^* = 0.86$.

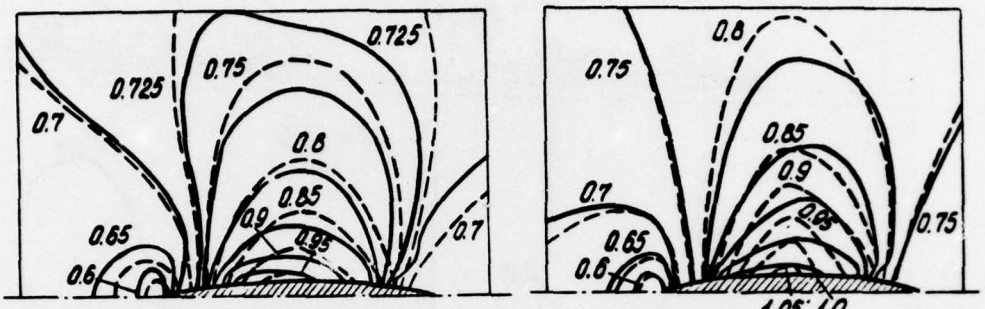

(a) $M_\infty = 0.725$ (b) $M_\infty = 0.761$

Fig. 36 Isotachs in transonic flow around a 12 per cent circular arc airfoil; calculated by the "large particles" method ——, ---- experiment of Wood and Gooderum [39].

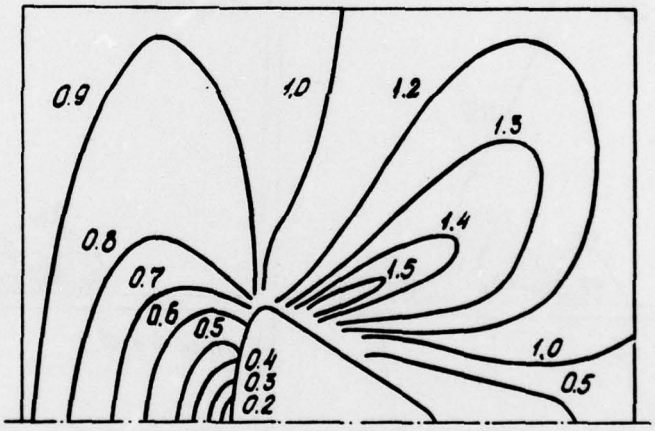

Fig. 37 Isotachs in sonic flow past a space vehicle of the Apollo type.

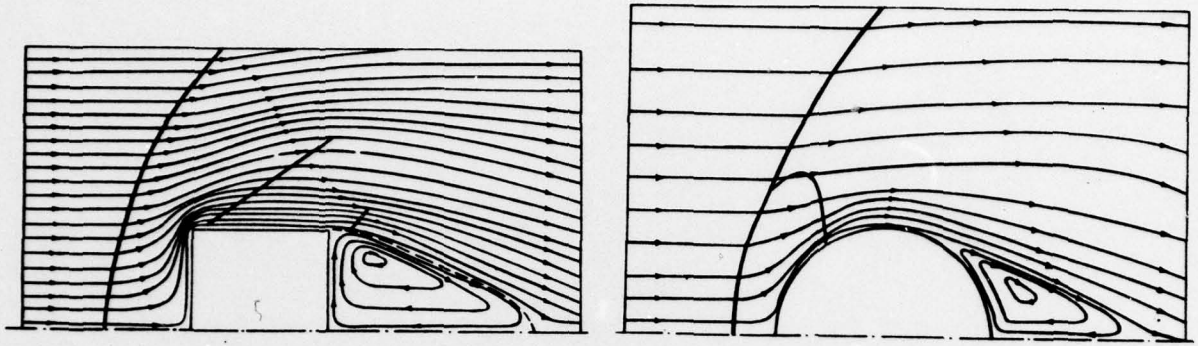

Fig. 38 Supersonic flow patterns around a short circular cylinder and a sphere, M = 2.0.

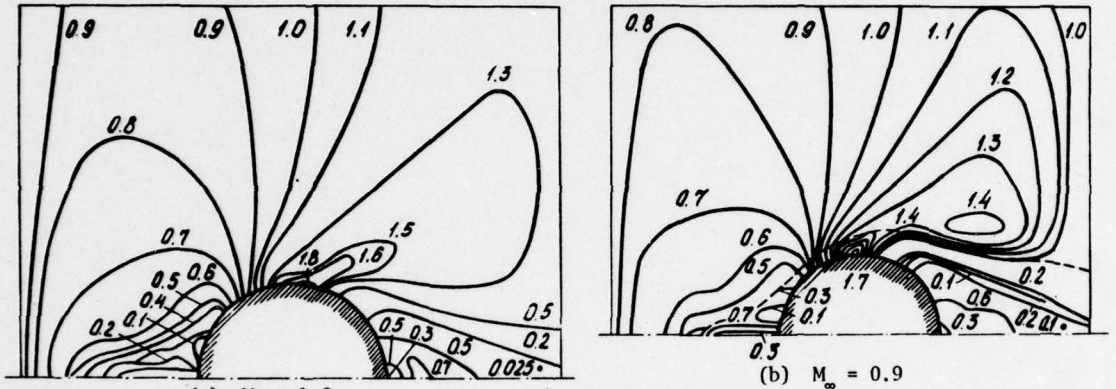

(a) $M_\infty = 1.0$ (b) $M_\infty = 0.9$

Fig. 39 Isotachs in transonic flow around a sphere with upstream injection on the body axis, $\rho_c = 2.9$ and $M_c = 1.0$, i.e., $u_c = -1.0$, $v_c = 0$.

SECURITY CLASSIFICATION OF THIS PAGE (When Data Entered)

REPORT DOCUMENTATION PAGE		READ INSTRUCTIONS BEFORE COMPLETING FORM
1. REPORT NUMBER AE-79-2	2. GOVT ACCESSION NO.	3. RECIPIENT'S CATALOG NUMBER
4. TITLE (and Subtitle) Investigation of Transonic Gas Flows (Analytical and Numerical Methods)		5. TYPE OF REPORT & PERIOD COVERED Final Technical
		6. PERFORMING ORG. REPORT NUMBER
7. AUTHOR(s) Oleg Belotserkovskii		8. CONTRACT OR GRANT NUMBER(s) N00014-79-M-0022
9. PERFORMING ORGANIZATION NAME AND ADDRESS The University of Maryland Aerospace Engineering Department College Park, Maryland 20742		10. PROGRAM ELEMENT, PROJECT, TASK AREA & WORK UNIT NUMBERS
11. CONTROLLING OFFICE NAME AND ADDRESS Department of the Navy Office of Naval Research Arlington, Virginia 22217		12. REPORT DATE March, 1979 13. NUMBER OF PAGES 61
14. MONITORING AGENCY NAME & ADDRESS(if different from Controlling Office)		15. SECURITY CLASS. (of this report) Unclassified 15a. DECLASSIFICATION/DOWNGRADING SCHEDULE

16. DISTRIBUTION STATEMENT (of this Report)

Approved for public release, distribution unlimited.

17. DISTRIBUTION STATEMENT (of the abstract entered in Block 20, if different from Report)

18. SUPPLEMENTARY NOTES

19. KEY WORDS (Continue on reverse side if necessary and identify by block number)

Transonic Flows; Blunt Body Flows; Method of Integral Relations; Large Particles Method; Domains of Dependence.

20. ABSTRACT (Continue on reverse side if necessary and identify by block number)

This report considers some problems of transonic gasdynamics related to the theory of planar and three-dimensional flows of a perfect gas which have been worked out mainly by the author and his collaborators. Results of analytical investigations of a number of exact properties of solutions which describe the flow around bodies with a detached shock, obtained by E.G. Shifrin, O.M. Belotserkovskii, et al., are presented without proof in the form of theorems (proofs are to be found in the papers cited). Results

next page

DD FORM 1 JAN 73 1473 EDITION OF 1 NOV 65 IS OBSOLETE
S/N 0102-LF-014-6601

SECURITY CLASSIFICATION OF THIS PAGE (When Data Entered)

Block number 20 continued.

of numerical solutions (due to O.M. Belotserkovskii, Yu M. Davidov, F.D. Popov, et al.), obtained by the methods of integral relations and "large particles", are presented for the complete problem of transonic flow around blunt bodies whose profiles possess sharp corners. The boundaries of distinct minimal domains of influence in mixed flow about blunt bodies are also examined.